

# Sources of Submicrometre Particles Near a Major International Airport

**Mauro Masiol<sup>1,2</sup>, Roy M. Harrison<sup>1\*†</sup>,  
Tuan V. Vu<sup>1</sup>, David C.S. Beddows<sup>1</sup>**

**<sup>1</sup> Division of Environmental Health and Risk Management,  
School of Geography, Earth and Environmental Sciences  
University of Birmingham  
Edgbaston, Birmingham B15 2TT  
United Kingdom**

**<sup>2</sup> Division of Epidemiology, Department of Public Health  
Sciences, University of Rochester Medical Center,  
265 Crittenden Boulevard, CU 420644  
Rochester, NY 14642, United States**

---

\* To whom correspondence should be addressed.

Tele: +44 121 414 3494; Fax: +44 121 414 3709; Email: r.m.harrison@bham.ac.uk

†Also at: Department of Environmental Sciences / Center of Excellence in Environmental Studies, King Abdulaziz University, PO Box 80203, Jeddah, 21589, Saudi Arabia

31    **ABSTRACT**

32    The international airport of Heathrow is a major source of nitrogen oxides, but its contribution to  
33    the levels of submicrometre particles is unknown, and is the objective of this study. Two sampling  
34    campaigns were carried out during warm and cold seasons at a site close to the airfield (1.2 km).  
35    Size spectra were largely dominated by ultrafine particles: nucleation particles (<30 nm) were found  
36    to be ~10 times higher than those commonly measured in urban background environments of  
37    London. Five clusters and 6 factors were identified by applying *k*-means cluster analysis and  
38    positive matrix factorization (PMF) respectively to particle number size distributions; their  
39    interpretation was based on their modal structures, wind directionality, diurnal patterns, road and  
40    airport traffic volumes and on the relationship with weather and other air pollutants. Airport  
41    emissions, fresh and aged road traffic, urban accumulation mode and two secondary sources were  
42    then identified and apportioned. The fingerprint of Heathrow has a characteristic modal structure  
43    peaking at <20 nm and accounts for 30-35% of total particles in both the seasons. Other main  
44    contributors are fresh (24-36%) and aged (16-21%) road traffic emissions and urban accumulation  
45    from London (around 10%). Secondary sources accounted for less than 6% in number  
46    concentrations but for more than 50% in volume concentration. The analysis of a strong regional  
47    nucleation event showed that both the cluster categorisation and PMF contributions were affected  
48    during the first 6 hours of the event. In 2016, the UK government provisionally approved the  
49    construction of a third runway; therefore the direct and indirect impact of Heathrow on local air  
50    quality is expected to increase unless mitigation strategies are applied successfully.

51

52    **Keywords:** Airport; black carbon; size distributions; source apportionment; ultrafine particles

53

54

## 55     **1.         INTRODUCTION**

56     Emerging markets, developing economies and globalisation have driven a fast and continuing  
57     growth of civil aviation in the last decades (Lee et al., 2009); this trend is still growing by ~5.5% y<sup>-1</sup>  
58     (ICAO, 2017). As a consequence, the aircraft and road traffic at airports is also increasing, but the  
59     information available on the impact of airport emissions upon air quality at ground level is still  
60     inadequate (Webb et al., 2008; Masiol and Harrison, 2014). The quantification of airport impacts on  
61     local air quality is complicated by the complexity of multiple mobile and static emission sources,  
62     with many airports being located near to major cities, highways or industrial plants. Consequently,  
63     the development of successful strategies for emission mitigation and the implementation of  
64     measures for air quality improvement to meet regulatory standards require a detailed quantification  
65     of the contribution of airport and other emissions to the total air pollution load.

66  
67     Biological evidence associates the exposure to ultrafine particles (UFPs, <100 nm) with adverse  
68     effects upon human health (e.g., Knibbs et al., 2011; Strak et al., 2012; Ostro et al., 2015; Lanzinger  
69     et al., 2016). At the current time, there is still limited knowledge of what specific characteristic or  
70     association of characteristics may dominate the particle toxicity, and the consequent health  
71     outcomes (Atkinson et al., 2010; Strak et al., 2012, Vu et al., 2015a); nevertheless it is well  
72     recognised that UFPs can reach the deepest regions of the lung (Salma et al., 2015) and may have  
73     orders of magnitude higher surface area to mass ratios compared to larger particles. They offer  
74     more surface for the absorption of volatile and semi-volatile species (Kelly and Fussell, 2012; Strak  
75     et al., 2012).

76  
77     Several studies have reported large increases of UFPs near airports (e.g., Westerdahl et al., 2008;  
78     Hu et al., 2009; Klapmeyer et al., 2012; Hsu et al., 2012a;b). For example, Hsu et al. (2013) and  
79     Stafoggia et al. (2016) detected substantial increases of total particle number concentration (PNC) at  
80     the airports of Los Angeles (CA, USA) and Rome Ciampino (Italy), respectively, in the few

81 minutes after take-offs, especially downwind, while landings made only a modest contribution to  
82 ground-level PNC observations. Hsu et al. (2014) observed that departures and arrivals on a major  
83 runway of Green International Airport (Warwick, RI, USA) had a significant influence on UFP  
84 concentrations in a neighborhood proximate to the end of the runway. In a study carried out at the  
85 Los Angeles international airport (CA, USA), Hudda et al. (2014) concluded that emissions from  
86 the airport increase PNC by 4- to 5-fold at 8–10 km downwind of the airfield, while  
87 Shirmohammadi et al. (2017) reported that the daily contributions of the airport to PNC were  
88 approximately 11 times greater than those from three surrounding freeways. Hudda et al. (2016)  
89 reported that average PNC were 2- and 1.33-fold higher at sites 4 and 7.3 km from the Boston (MA,  
90 USA) airport when winds were from the direction of the airfield compared to other directions.  
91  
92 Despite the strong evidence that airports are major sources of UFPs, their fingerprint within the  
93 particle number size distribution (PNSD) may be difficult to identify due to: (i) the nature of semi-  
94 volatile compounds emitted by aircraft; (ii) the possible mechanisms of secondary aerosol  
95 formation; (iii) the dilution effect; and (iv) the similar modal structures of other emission sources  
96 concurrently found in cities, such as road traffic (Masiol and Harrison, 2014). Generally, studies  
97 performed within or close to airports have reported increases of particles ranging from 4 to 100 nm  
98 in diameter and mostly distributed in the nucleation range ( $<30$  nm). For example, Mazaheri et al.  
99 (2009) showed a main nucleation mode and an accumulation mode (40–100 nm) more evident  
100 during take-offs; Keuken et al. (2015) reported PNSD dominated by 10–20 nm particles in an area  
101 affected by emissions from Schiphol airport (The Netherlands); Hudda and Fruin (2016) found  
102 strong increases in particles smaller than 40 nm downwind from the Los Angeles International  
103 Airport; Ren et al. (2016) showed that particles peaking at 16 nm dominate the PNSD at various  
104 distances from the runway of Tianjin International Airport, China; Masiol et al. (2016) reported that  
105 the fingerprint of aircraft emissions sampled under real ambient conditions at the airport of Venice  
106 (Italy) has a main mode at approx. 80 nm and a second mode in the nucleation range below 14 nm.

107

108 The Greater London area is home to more than 8.5 million inhabitants and is one of the few UK  
109 locations not fully achieving the EU and national air quality standards: in 2015 nitrogen dioxide  
110 breached the hourly and annual limit values for health, while ozone exceeded the long-term  
111 objective (DEFRA, 2016). However, the standards were fully met for both PM<sub>10</sub> and PM<sub>2.5</sub>.

112

113 London Heathrow (LHR) is one of the world's busiest international airports: it is ranked 1st in  
114 Europe for total passenger traffic (ACI, 2016). It accommodates more than 1250 flights every day  
115 and serves a total of 72.3 million passengers year<sup>-1</sup>. LHR is composed of 5 terminals and 2 runways:  
116 northern (3.9 km-long) and southern (3.7 km). Currently, runways operate near their maximum  
117 capacity, with a consequent increase in the potential for delays when flights are disrupted. Since  
118 2007, the proposal for expanding LHR with a 3rd runway and a 6th terminal has been intensely  
119 debated in the UK. In 2016 the UK government provisionally approved the construction of a third  
120 runway (UK Department for Transport, 2017).

121

122 LHR is located west of London (Figure SI1). Consequently, air quality in the surroundings of the  
123 airport may be affected by the advection of air masses from the city, with the associated high levels  
124 of pollutants emitted from traffic, energy demand for domestic heating and local industries. Airport  
125 activities may also contribute to air pollution advected to the city when LHR is upwind, with  
126 consequent potential impacts upon public health. In addition, as LHR attracts a large number of  
127 passengers and workers, the emissions from large volumes of road traffic generated by the airport  
128 and the nearby M4 and M25 motorways are difficult to discriminate from non-airport-related road  
129 traffic. Due to this complex scenario, the contribution of LHR is difficult to differentiate from the  
130 urban background pollution, as already reported by previous modelling and experimental studies  
131 (Farias and ApSimon, 2006; Masiol and Harrison, 2015).

132

133 Various studies have attempted to quantify the effect of LHR upon air quality, mainly focusing on  
134 the nitrogen oxides ( $\text{NO}_x = \text{NO} + \text{NO}_2$ ), which are well-known tracers for aircraft engine exhausts  
135 (e.g., Herndon et al., 2008; Masiol and Harrison, 2014 and references therein), but also arise from  
136 other combustion sources. For example, Carslaw et al. (2006) estimated that airport operations in  
137 2001/4 accounted for ~27% of the annual mean  $\text{NO}_x$  and  $\text{NO}_2$  at the airfield boundary and less than  
138 15% ( $<10 \mu\text{g m}^{-3}$ ) at background locations 2-3 km downwind of the airport. Similar results were  
139 found for the 2008/9 period using model evaluation (AEA, 2010) and for the 2005/12 period using  
140 experimental data analysis (Masiol and Harrison, 2015). This latter study also reported that PM  
141 mass concentrations at eight sites all around LHR were always well below the EU and UK limit.

142  
143 This study aims to investigate the impacts of a major airport (LHR) serving a megacity (London)  
144 upon the levels of submicrometre particles and to apportion those impacts to aircraft, road traffic  
145 and other sources typical of large cities with airports. The main particle size distributions modes are  
146 simplified by applying cluster analysis; then, the modal structures of the main potential sources are  
147 disaggregated and the submicron particle number concentrations (PNC) are quantified through the  
148 positive matrix factorisation (PMF). In addition, the origin of the airport plumes was spatially  
149 assessed by matching results with local meteorological data, air mass movements, levels of  
150 common air pollutants,  $\text{PM}_{2.5}$  mass concentration and its chemical speciation as indicators of source  
151 location and formation mechanisms.

152  
153 The atmospheric chemistry and physical properties of UFPs have been extensively investigated in  
154 London (e.g., Harrison et al., 2012; Jones et al., 2012; von Bismarck-Osten et al., 2013) with  
155 several studies using cluster analysis (Beddows et al., 2009; Brines et al., 2014; 2015) or PMF  
156 (Beddows et al., 2015; Vu et al., 2016). However, this study is the first one carried out in South-  
157 West London to characterise and quantitatively apportion the impacts of LHR under real ambient  
158 conditions. Moreover, only one earlier study (Masiol et al., 2016) has used both cluster analysis and

159 PMF to directly assess the airport contributions to UFPs. In addition, this study also investigated the  
160 effects of a regional nucleation event on the results of the two source apportionment methods.

161

## 162 **2. MATERIALS AND METHODS**

### 163 **2.1 Experimental**

164 Two sampling campaigns (each 1 month-long) were carried out during warm (August-September  
165 2014) and cold (December 2014-January 2015) periods at Harlington (Figure SI1). The site was  
166 selected as well located to sample the plumes from the airport emissions: it lies 1.2 km N of the  
167 northern runway and is located inside a playground, close to a secondary road and near the village  
168 of Harlington. This is the location selected for the construction of the 3rd runway. The site is  
169 categorised as “urban industrial” by DEFRA and it is therefore more indicative of community  
170 exposure rather than direct fresh aircraft emissions. Consequently, it is a good point to quantify the  
171 particles generated by the airport after a relatively short ageing and dispersion in the atmosphere,  
172 and is more indicative of the fingerprint of aircraft emissions affecting communities than data  
173 collected alongside the runway or in the airport apron areas. In addition, previous studies have  
174 reported that the site is strongly affected by the plume from the airport (Carslaw et al., 2006; Masiol  
175 and Harrison, 2015). Prevailing winds from the 3rd and 4th quadrants are recorded in both summer  
176 and winter (Figure SI2): under such circulation regimes, Harlington lies just downwind of LHR.  
177 The site is also affected by pollutants arising from the large volumes of road traffic within London,  
178 from the local road network as well as those generated by the airport. Tunnel Rd., the main access  
179 to LHR from the M4 motorway lies 800 m west, as well as the nearby M4 (640 m north) and M25  
180 (~3.5 km east) motorways, major roads (Bath Rd, part of A4, passes 900 m south; A30 lies 2.8 km  
181 SE). The village of Harlington (~400 m west) and advection of air masses from the conurbation of  
182 London are other potential external sources.

183

184 Ultrafine particle counts and their size distributions from 14.3 to 673.2 nm were measured at 5 min  
185 time resolution using a SMPS (scanning mobility particle sizer spectrometer) comprising an  
186 electrostatic classifier TSI 3080 with a long differential mobility analyser (TSI 3081) and a CPC  
187 (condensation particle counter, TSI 3775) based on condensation of *n*-butyl alcohol (Fisher  
188 Scientific, ACS). The SMPS operated at a sheath air to aerosol flow ratio of 10:1 (sheath and  
189 sample air flow rates were 3.0 and 0.3 L min<sup>-1</sup> respectively, voltage 10-9591 V; density 1.2 g/cc;  
190 scan time 120 s, retrace 15 s; number of scan 2) while the CPC operated at low flow rate (0.3 L  
191 min<sup>-1</sup>). The use of 5 min resolved spectra has already been used successfully for source  
192 apportionment purposes at an airport (Masiol et al., 2016).

193

194 Equivalent Black Carbon (eBC) as defined by Petzold et al. (2013) was also measured at 5 min  
195 resolution using a 7-wavelength aethalometer (Magee Scientific AE31). The aethalometer operated  
196 with an inlet cut-off head to collect PM with aerodynamic diameter of <2.5 µm (PM<sub>2.5</sub>). eBC was  
197 derived from the absorbance at 880 nm wavelength (Petzold et al., 2013); raw data were post-  
198 processed with the Washington University Air Quality Lab AethDataMasher V7.1 to perform data  
199 validation and correct data for non-linear loading effects (Virkkula et al., 2007; Turner et al., 2007).

200

201 Instruments were installed into a plastic/metal case designed for sampling purposes: (i) air inlets  
202 were ~1.8 m above the ground and were composed of conductive materials to avoid particle losses  
203 and sampling artefacts; (ii) the case was cooled by fans in summer and was warmed by an electrical  
204 tubular heater in winter for maintaining an indoor air temperature within an acceptable range for  
205 running the equipment (temperature inside the case was recorded and periodically checked); (iii)  
206 instruments were isolated from vibration using rubber pads and foam foils. Devices were fully  
207 serviced, calibrated by authorised companies and underwent internal cross-calibrations with other  
208 similar instruments under lab conditions. Moreover, frequent periodic checks, maintenance of  
209 instruments and cleaning of inlets was performed throughout the sampling campaign.



210

211 Routine air pollutants (NO, NO<sub>2</sub>, NO<sub>x</sub>, O<sub>3</sub>, PM<sub>10</sub>, PM<sub>2.5</sub>) were measured at Harlington with 1 h time  
212 resolution by the UK Automatic Urban and Rural Network under the auspices of the UK  
213 Department for Environment, Food and Rural Affairs (DEFRA; <http://uk-air.defra.gov.uk/>).  
214 Gaseous species were analysed using automatic instruments according to European standards and  
215 National protocols: EN 14211:2012 for nitrogen oxides and EN 14625:2012 for ozone. PM<sub>10</sub> and  
216 PM<sub>2.5</sub> were analysed using tapered element oscillating microbalance and filter dynamics  
217 measurement system (TEOM-FDMS) to provide measurements accounting for volatile (VPM<sub>10</sub>,  
218 VPM<sub>2.5</sub>) and non-volatile (NVPM<sub>10</sub>, NVPM<sub>2.5</sub>) fractions. Quality assurance and quality control  
219 procedures followed the standards applied for the Automatic Urban and Rural Network (AURN)  
220 and the London Air Quality Network (LAQN). Instruments were routinely calibrated, and every six  
221 months were fully serviced and underwent intercalibration audits.

222

223 Some additional variables are also computed from the air pollutants to help the interpretation of  
224 results. The NO<sub>2</sub>/NO<sub>x</sub> ratio is indicative of the partitioning of nitrogen oxides, while the levels of  
225 oxidants (OX=O<sub>3</sub>+NO<sub>2</sub>, expressed in ppbv) can be used to roughly assess the oxidative potential in  
226 the atmosphere (Kley et al., 1999; Clapp and Jenkin, 2001). These two new variables are useful in  
227 investigating the atmospheric chemistry behind the NO-NO<sub>2</sub>-O<sub>3</sub> system. Delta-C (the difference  
228 between absorbance at 378 and 880 nm, also called UVPM) was also computed. This variable was  
229 largely used as a proxy to estimate the fraction of carbonaceous material emitted by biomass  
230 burning (e.g., Sandradewi et al., 2008; Wang et al., 2011). However, Delta-C results should be used  
231 with caution: Harrison et al. (2013) showed that there are probably other UV absorbing contributors  
232 than wood-smoke to the aethalometer signal. Consequently, Delta-C is used here only for  
233 qualitative purposes.

234

235 Weather data were measured hourly by the Met Office at LHR; met data include wind direction and  
236 speed, atmospheric pressure, air temperature, relative humidity (RH), visibility, rain and solar  
237 irradiance.

238

239 During the two campaigns, 24-h PM<sub>2.5</sub> samples were also collected on quartz filters using a high  
240 volume air sampler (TE-6070, Tisch Environmental, Inc.) and analysed for the daily concentrations  
241 of major PM<sub>2.5</sub> components: organic carbon (OC) and elemental carbon (EC) by thermo-optical  
242 analysis (EUSAAR\_2 protocol) and major inorganic ions (Na<sup>+</sup>, K<sup>+</sup>, ammonium, nitrate, sulphate,  
243 oxalate) by ion chromatography. Analytical methods are reported in detail in Yin et al. (2010). The  
244 results of the chemical speciation of PM<sub>2.5</sub> are presented in a companion paper (in preparation) and  
245 are used in this study only to assist the interpretation of PMF results.

246

## 247 **2.2 Data Handling and Chemometric Approaches**

248 Data were analysed using R version 3.3.1 (R Core Team, 2015) and a series of supplementary  
249 packages, including ‘Openair’ (Carslaw and Ropkins, 2012). Preliminary data handling and clean-  
250 up were carried out to check the robustness of the dataset, detect anomalous records and to delete  
251 extreme outliers. SMPS data with unreliable behaviour or instrument errors were completely  
252 deleted. An in-depth analysis of the dataset revealed few records with anomalously high PNC,  
253 which were likely related to probable instrumental issues, extreme weather conditions (e.g., high  
254 wind gusts, heavy rain striking the inlet), or infrequent local emissions, e.g., maintenance, painting  
255 and recreational activities (including fires) on the playground where the site is located, road  
256 maintenance close the site and probable short-term parking of high-emission vehicles near the site.  
257 Since this study aims to investigate the overall contributions of LHR, all data are used for  
258 descriptive statistics, but data greater than the 99.5th percentile were further removed for  
259 explorative, cluster and PMF analyses. This data exclusion successfully removed the extremely high  
260 events occurring during the sampling campaigns and significantly improved the stability and

physical meaning of PMF solutions. Missing data for other variables were linearly interpolated between the nearest values of the time series.

The particle number size distributions (PNSDs) were firstly grouped by applying a *k*-means cluster analysis. The full method is exhaustively discussed in Beddows et al. (2009; 2014) and aims to assemble single spectra into *k* clusters. The clustering groups observations with spectra similar to their cluster centroids (means), i.e. observations that are likely generated by the same set of formation processes or emission sources. The optimum number of clusters (*k*) was determined by an optimisation algorithm based on the spectral shapes (Beddows et al., 2009). The choice to apply the *k*-mean clustering method was based on several reasons: (i) Salimi et al. (2014) reported that *k*-means is the best performing clustering among others methods tested on PNSD data; (ii) *k*-means is a well-established method which has been widely applied over a number of different sites (e.g., Dall'Osto et al., 2012; Wegner et al., 2012; Beddows et al., 2014; Brines et al., 2014; 2015); and (iii) the method was previously applied successfully to airport data (Masiol et al., 2016).

PMF analysis was performed by applying the USEPA PMF5 model. Details of the PMF model are reported elsewhere (Paatero and Tapper, 1994; Paatero, 1997; USEPA, 2014), while the best practice and standards are extensively reviewed in several papers (e.g., Reff et al., 2007; Belis et al., 2014; Brown et al., 2015; Hopke, 2016). SMPS data at 5 min resolution were used as the PMF input matrix. Uncertainties associated with SMPS data were estimated according to the empirical method proposed by Ogulei et al. (2007). Uncertainty for the total variable (total particle number concentration, PNC) was set at 300% of the PNC concentration and also marked as “weak” to avoid it driving the profiles.

The best PMF solutions were identified: (i) by investigating solutions between 3 and 10 factors; (ii) by considering the minimization of the objective function *Q* with respect to the expected (theoretical) value and its stability over multiple (n=100) runs, (iii) by obtaining low values for the

287 sum of the squares of the differences in scaled residuals for each base run pair by species; (iv) by  
288 minimizing the number of absolute scaled residuals over  $\pm 3$  and by keeping them symmetrically  
289 distributed; (v) by keeping the result uncertainties calculated by bootstrap (BS,  $n=200$ ) and  
290 displacement (DISP) methods within an acceptable range (Paatero et al., 2014); (vi) by obtaining  
291 modelled total variable (PNC) successfully predicted ( $R^2 > 0.9$  and slopes  $\approx 1$ ); and (vii) by avoiding  
292 the presence of edges in the G-space plots (Paatero et al., 2002) and, then, the presence of  
293 hidden/unresolved sources.

294  
295 A series of additional tools were used to analyse the raw data, link source apportionment results to  
296 other variables, such as local atmospheric circulation and regional/transboundary transport of air  
297 masses. Briefly, polar plots aim to map pollutant average concentrations by wind speed and  
298 direction as continuous surfaces (Carslaw et al., 2006), while polar annuli plot by wind direction  
299 and hours of the day. The potential locations of distant sources were assessed using back-trajectory  
300 analysis and a concentration weighted trajectory (CWT) model (Stohl, 1998). Back-trajectories  
301 were computed with the HYSPLIT4 model (Stein et al., 2015; Rolph, 2016) using NCEP/NCAR  
302 reanalysis gridded meteorological data. Set-up: -96 h with a starting height of 500 m a.g.l. CWT is a  
303 method of weighting trajectories with associated concentrations to detect the most probable source  
304 areas of long-range transports of pollutants; it has been used and reviewed in a number of prior  
305 studies (e.g., Stohl, 1996; Lupu and Maenhaut, 2002; Squizzato and Masiol, 2015).

### 310 **3. RESULTS AND DISCUSSION**

#### 311 **3.1 Overview of Data**

312 The wind roses during the two sampling periods are provided in Figure SI2. Descriptive statistics of  
313 all collected variables are reported as boxplots in Figure SI3. PNSDs were initially split into 3  
314 ranges: nucleation (14-30 nm), Aitken nuclei (30-100 nm) and accumulation (>100 nm). On  
315 average the total PNC during the warm season was  $1.9 \times 10^4$  particles  $\text{cm}^{-3}$ , of which  $1.1 \times 10^4$ ,  $6.4 \times$   
316  $10^3$  and  $1.5 \times 10^3$  particles  $\text{cm}^{-3}$  were classified as nucleation, Aitken and accumulation ranges,  
317 respectively (Figure SI3). During the cold season, the total average PNC was  $2.2 \times 10^4$  particles  
318  $\text{cm}^{-3}$ , composed of  $1.4 \times 10^4$ ,  $6.3 \times 10^3$  and  $1.4 \times 10^3$  particles  $\text{cm}^{-3}$  as nucleation, Aitken and  
319 accumulation ranges, respectively (Figure SI3). Concentrations lie between those of London,  
320 Marylebone Road (kerbside) and London, North Kensington (background), and nucleation particles  
321 were ~10 times higher than the annual average measured in North Kensington as reported by Vu et  
322 al. (2016), while Aitken particles were 1.9 times higher. It is therefore evident that the main  
323 difference lies in the concentration of the finest size ranges: in both seasons, spectra were  
324 dominated by UFP ( $D_p < 100$  nm) particles (~92% of total PNC), which only accounted for ~12% of  
325 total particle volume concentration (PVC, computed by approximation to spherical particles). On  
326 the other hand, accumulation mode particles accounted for ~8% of PNC and ~88% of PVC volume.  
327 The high levels of total PNC are not surprising: several studies carried out into or close to airports  
328 (e.g., Hsu et al., 2013;2014; Hidda et al., 2014; 2016; Stafoggia et al., 2016; Shirmohammadi et al.,  
329 2017) reported significant increases in the concentrations of UFPs.

330

331 During the two sampling campaigns, air pollutants measured in Harlington (Figure SI3) were  
332 similar to the average concentrations measured over an 8 year period (2005-2012) in the vicinity of  
333 LHR (Masiol and Harrison, 2015). Consequently, despite the two short campaigns carried out in  
334 this study, results may be considered representative of the average levels of air pollution recorded at  
335 Harlington. The average concentrations of eBC were  $2.4$  and  $2.1 \mu\text{g m}^{-3}$  during the warm and cold  
336 season, respectively. The average concentration of Delta-C was  $0.1 \mu\text{g m}^{-3}$  during the warm season  
337 and  $0.36 \mu\text{g m}^{-3}$  in winter.

338

339 Analysis of the data showed a non-normal distribution for most of the variables: the nonparametric  
340 Kruskal-Wallis one-way analysis of variance was therefore used to test the difference of  
341 concentrations over the two periods (Kruskal and Wallis, 1952): almost all variables are different at  
342 the 0.05 significance level, except NO, NO<sub>x</sub> and O<sub>3</sub>. This result indicates a seasonal effect upon air  
343 quality in the LHR area and suggests investigating the sources over the two periods separately.

344

345 The average PNSDs are shown in Figure 1 as well as their median distributions and interquartile  
346 ranges. Spectra are categorised by time of day (7am-7pm and 7pm- 7am local time). In addition, the  
347 particle volume size distributions (PVSDs) are also provided. Results for the warm season show  
348 that the average daytime PNSD is dominated by a main peak in the nucleation range (extending  
349 below 14 nm) and a second mode in the Aitken range (between 30 and 50 nm). The nocturnal  
350 spectrum is characterised by a drop of the nucleation mode to concentration values similar to the  
351 Aitken peak (mode around 35 nm). During the cold season, the average diurnal and nocturnal  
352 PNSDs present a main peak at 15-25 nm and a second mode at 70-100 nm. In summary, both  
353 seasons show reductions of the finest modes during nighttime, while the second mode is almost  
354 constant throughout the day. As a consequence, the modal structure of PNVDs is also almost  
355 constant throughout the day.

356

357 The diurnal cycles of the 3 particle ranges, eBC, solar irradiation and airport movements are shown  
358 in Figure 2. A comprehensive overview of the patterns for all the variables is provided in Figure  
359 SI4. Generally, diurnal cycles derive from the interplay of emissions, dispersion and atmospheric  
360 chemical processes. Consequently, they need to be investigated along with patterns for airport and  
361 motorway traffic (Figure 2 and Figure SI5, respectively), and as polar annuli (Figures SI6 and SI7)  
362 and polar plots (Figures SI8 and SI9), which give preliminary insights into the origin and spatial  
363 location of most probable emission sources. During nighttime, airport traffic is restricted to limit

364 noise and community disturbance: flights are generally constant from 6 am to 8 pm and are kept at  
365 minimum overnight, with no departures normally scheduled between 11 pm and 6 am (Figure 2).  
366 Road traffic is more difficult to define. Data for M4 and M25 motorways are provided by the UK  
367 Department for Transport: data for the M4 motorway show typical morning (7-8 am) and evening  
368 (5-6 pm) peaks due to rush hours, but this pattern is not well-resolved for the M25 (Figure SI5). In  
369 addition, despite it being likely that traffic on minor and local roads also follows patterns dominated  
370 by rush hours, traffic generated by the airport is more difficult to characterise, with Tunnel Rd. and  
371 other busy roads serving LHR being frequently congested.

372

373 Nucleation particles are likely associated with aircraft movements. The daily pattern shows high  
374 and almost constant concentrations between 7 am and 11 pm (Figure 2): hourly averages ranged  
375 from  $10 \times 10^3$  to  $15 \times 10^3$  particles  $\text{cm}^{-3}$  during the warm season and from  $10 \times 10^3$  to  $21 \times 10^3$   
376 particles  $\text{cm}^{-3}$  during the cold season. On the contrary, the concentrations of nucleation particles  
377 significantly (Kruskal-Wallis at  $p < 0.05$ ) drop overnight (hourly averages ranging from  $5 \times 10^3$  to  
378  $6 \cdot 10^3$  particles  $\text{cm}^{-3}$  and from  $1 \times 10^3$  to  $5 \cdot 10^3$  particles  $\text{cm}^{-3}$  during the warm and cold season,  
379 respectively); the maximum average concentrations are recorded for winds blowing from the SW  
380 quadrant (polar plots and polar annuli in Figures SI6-9), i.e. the airfield and, in particular, the  
381 location of the main LHR terminals (Figure SI1). As a consequence of the dominance of nucleation  
382 particles over size spectra, also total PNC follows the pattern (Figures 2) and wind directionality  
383 (Figures SI8-9) of nucleation particles. On the contrary, accumulation particles appear to be more  
384 associated with road traffic. These particles increase for winds blowing from northern sectors  
385 (Figures SI6-9), i.e. toward the M4. Accumulation particles also present the morning (6-8 am) and  
386 evening (6-11 pm) rush hour peaks during the warm season, but only the evening peak (from 6 pm  
387 to the night) was found in the cold season (Figure 2). Generally, the evening peaks start around 6  
388 pm, which is consistent with the peak of traffic (Figure SI5) but they extend late in the evening and  
389 night probably because the drop of the mixing layer top and the consequent concentration of

390 pollutants close to the ground level. Aitken nuclei exhibit a mixed behaviour between nucleation  
391 and accumulation particles (Figure 2): two different patterns can be found, which are more  
392 consistent with road traffic in summer and with aircraft traffic in winter.

393

394 Despite some studies indicating that airports are strong sources of black carbon (Dodson et al.,  
395 2009), other studies report no strong relationships with the flight activity (Masiol et al., 2016; Hsu  
396 et al., 2016). Similarly to NO<sub>2</sub> (Figure SI4) and accumulation particles (Figure 2), aethalometer data  
397 also shows typical patterns of road traffic-influenced sites for all wavelengths, with two daily peaks  
398 corresponding to the hours with higher traffic (Figure 2). However, Delta-C does not present any  
399 evident pattern (Figure SI4). eBC shows increased concentrations when winds blow from northern  
400 sectors (plus SE in winter, Figure SI7 and SI9); which excludes airport activities as being a  
401 dominant source in the study area.

402

403 Particulate matter mass concentration (PM<sub>10</sub> and PM<sub>2.5</sub>) has very weak diurnal patterns (Figure SI4).  
404 Its wind directionality shows evident increases for northerly winds (Figure SI8-9). It is therefore  
405 evident that PM mass concentrations are dominated by non-airport sources, i.e. regional secondary  
406 pollutants, traffic from the nearby M4 or background pollution from London. PM<sub>2.5</sub> concentrations  
407 normally do not exceed the Limit Values in the Greater London area (DEFRA, 2016).

408

### 409 **3.2 *k*-means Cluster Analysis**

410 The clustering algorithm extracted 5 clusters for both periods. The number of clusters was selected  
411 according to the optimisation algorithm, i.e. local maxima in the Dunn indices and silhouette  
412 (Beddows et al., 2009). The extraction of 5 clusters represents a good compromise for the  
413 interpretation of spectral observations. Hussein et al. (2014) reported that is not prudent to describe  
414 the spectra with few clusters (2-4), which are not sufficient to explain variations and detailed



415 differences in the PNSD observed in the urban atmosphere. On the other hand, they also reported  
416 that extracting too many ( $>10$ ) clusters may make the aerosol source attribution more challenging.  
417

418 The cluster centroids (mean spectra of each cluster), the 10th, 25th, 75th and 90th percentile, the  
419 hourly counts patterns and resulting wind roses are shown in Figures 3 and 4 for the warm and cold  
420 season campaigns, respectively. Despite extracted clusters exhibiting significantly different modal  
421 structures for PNC, no differences can be observed for the particle volume size spectra, which all  
422 show a unimodal peak at approx. 200-300 nm. Clusters accounted for 14%-25% of total  
423 observations for both the seasons: Table SI1 summarises the percentage of the total observations for  
424 each cluster.

425

426 Three clusters (*cluster 1* during the warm season and *clusters 1 and 5* in winter) are likely shaped  
427 by the airport emissions. The modal structures present sharp peaks for nucleation particles which  
428 extend below the SMPS detection limit (14 nm) and drop at 30-40 nm; no secondary modes are  
429 present in the Aitken or accumulation ranges. These clusters show a large increase in frequency  
430 during the afternoon and evening hours (cluster 1 for the warm season and cluster 5 for the cold  
431 season) or extended over the daytime (cluster 1 for the cold season), similarly to the airport aircraft  
432 movement profiles (Figure 2). Aircraft are known to emit particles in the nucleation range (e.g.  
433 Mazaheri et al., 2009;2013; Masiol and Harrison, 2014; and references therein; Lobo et al., 2015)  
434 and the wind roses are also compatible with an origin from the airfield and the main LHR terminals  
435 (Figures 3 and 4). However, daytime regional photochemical nucleation events in London occur  
436 around noon-2 pm and are mostly recorded from June to September (Vu et al., 2016).

437 Consequently, the modal structure of cluster 1 for the warm season could be additionally shaped by  
438 regional photochemical nucleation. The reasons driving the split of the spectra likely shaped by  
439 LHR into two clusters during the cold season are unclear. A further comparison of the cluster and  
440 PMF results will help in interpreting this outcome.

441

442 The modal structures of the *clusters 4* for both seasons peak for nucleation particles and extend  
443 below 14 nm, but also show probable modes between 50 and 200 nm (Figures 3 and 4). They  
444 represent the typical spectra associated with aged anthropogenic emissions, mostly due to road  
445 traffic. It is recognised that road traffic contributes to a large range (30-200 nm) of PNSD in the  
446 urban atmosphere (e.g., Yue et al., 2008; Costabile et al., 2009; Harrison et al., 2011), which is  
447 compatible with these spectra. The directional analysis for the warm season shows increased levels  
448 when air masses move from the sectors more affected by traffic, i.e. London (NE), M4 (N) and M25  
449 (W) motorways and Tunnel Rd (W), while the hour count profile presents a huge maximum during  
450 daytime. In winter, this modal structure mostly occurred for westerly winds: the atmospheric  
451 circulation during the cold season mostly experienced winds blowing from the SW quadrant, with  
452 NE sectors poorly represented (Figure SI1). As a consequence, the limited number of observations  
453 for air pollution advected from the Greater London area may have affected the detection of the  
454 urban background from London. This lack of data is also reflected by diurnal profile, which shows a  
455 marked peak in the late afternoon, concurrent to the peak of traffic on M4 and M25 (Figure SI5).

456

457 Three clusters (*clusters 2* and *3* during the warm season and *cluster 2* in winter) exhibited similar  
458 hourly profiles with most of the counts occurring overnight (Figures 3 and 4). This pattern is largely  
459 attributable to the dynamics of the mixing layer, since the diurnal cycles are the mirror image of the  
460 ambient air temperature (Figure SI4). Because of this, these clusters could be potentially affected by  
461 the reduced height of the mixing layer occurring overnight. These clusters exhibit bimodal  
462 structures with the coarser modes with respect to the remaining clusters: cluster 2 for the warm  
463 season shows a main peak in number concentrations at 30-40 nm and a second peak in the finest  
464 range (<16 nm), clusters 3 for the warm season peaks at 14 and 60-70 nm, and cluster 2 for the cold  
465 season extends over a wide size range with two modes around 20-30 nm and 100-150 nm.

466 Consequently, these clusters are likely representative of spectra mostly shaped by the drop of the

467 mixing layer height and the formation of secondary aerosols. In this context, the potential role of  
468 nighttime nitrate formation through condensation of  $\text{NH}_4\text{NO}_3$  and the heterogeneous reactions of  
469  $\text{N}_2\text{O}_5$  and  $\text{NO}_3$  on pre-existing particles cannot be ignored (Seinfeld and Pandis, 2006; Bertram and  
470 Thornton, 2009; Brown and Stutz, 2012). The wind roses reveal that both clusters 2 occur under  
471 similar westerly wind regimes. Regional aerosols appear to be the most probable source. On the  
472 contrary, cluster 3 for the warm season occurs with winds from London (NE) and likely represents  
473 particle size spectra mainly shaped by primary and secondary aerosols advected from the most  
474 urbanised areas, i.e. it is most likely associated with the urban background of London.

475

476 *Cluster 5* for the warm season and *cluster 3* for the cold season may be associated with road traffic.  
477 They reveal modal structures with a dominant peak around 20-35 nm (cluster 5 also shows a  
478 possible second peak at 15 nm) and mostly occur when air masses blow from westerly sectors,  
479 which are compatible with the location of motorways and Tunnel Rd, the main roadway linking  
480 LHR to the M4 motorway. In summer, the hourly count pattern exhibits two maxima (6-8 am and 4-  
481 8 pm) related to morning and evening rush hours; this pattern is compatible with fresh road traffic  
482 emissions. However, the diurnal pattern in winter also presents a high number of counts at 3-5 am,  
483 i.e. not directly compatible with rush hours. A possible explanation involves the stronger effect of  
484 the winter mixing layer dynamics on the air quality due to the presence of more frequent low level  
485 thermal inversions, which may build up the pollutants at ground-level especially overnight. This  
486 may increase the signal of the less intense, but still significant, nighttime traffic emissions present in  
487 the study area.

488

489

490

### 491 **3.3 PMF Analysis**

492 The interpretation of PMF results was then attempted by considering: (i) the knowledge of sources  
493 impacting the study area; (ii) the comparison with the results reported by Vu et al. (2016), who  
494 performed a PMF analysis of SMPS data collected in North Kensington (London urban  
495 background); (iii) the shape of resulting profiles for both the particle number and volume  
496 concentrations; (iv) the analysis of diurnal patterns; (v) the directional analysis using the polar plot  
497 and polar annuli; (vi) the correlations between the source contributions and the other air pollutants  
498 monitored at the site or with weather variables, and (vii) the analysis of possible remote source  
499 areas by applying the CWT model.

500

501 Six-factor solutions were extracted for both the seasons. The resulting factor profiles are presented  
502 in Figures 5 and 6 for the warm and cold season, respectively. The factor profiles are expressed as:  
503 (i) particle number concentrations and their DISP ranges; (ii) particle volume concentrations, and  
504 (iii) explained variations showing how much of the variance (from 0 to 1) in the original dataset is  
505 accounted for by each extracted factor. The Figures 5 and 6 also show the diurnal patterns and the  
506 polar plots computed from the hourly-averaged contributions. Table 1 summarises the PMF results  
507 and spectral characteristics, while Table 2 shows the Pearson correlation matrices with weather and  
508 air quality variables. Selected PMF solutions were very stable: no errors or unmapped factors and  
509 few swaps (none in summer and <7% in winter) were found in BS; no swaps or errors even at  
510  $dQ_{max}=25$  were found for DISP, i.e. solutions were affected by small rotational ambiguity and,  
511 therefore, their interpretation can be considered robust.

512

513 DISP analysis is designed to explore the realistic bounds on the optimal (base run) PMF solutions  
514 that do not result in appreciable increases in the  $Q$  values (Brown et al., 2015). In this study, the  
515 ranges calculated by DISP for the  $dQ=4$  were used to assess the uncertainty boundaries associated  
516 with the final PMF profiles, as suggested in Zikova et al. (2016) and Masiol et al. (2017). This

strategy is useful to better interpret the results, as the regions of spectra affected by high rotational ambiguity are disclosed in the resulting profiles.

### 3.3.1 Warm season

*Factor 1* includes most of the particles in the nucleation range (<20 nm), exhibits a sharp mode in the number distribution below the SMPS detection limit (14 nm) and makes the largest contribution to the total PNC (31.6%, DISP range 31-36%) (Figure 5). However, its contribution to the volume distribution is ~1%. Several studies report that particles in the nucleation range are emitted from aircraft engines (e.g., Anderson et al., 2005; Herndon et al., 2008; Kinsey et al., 2010; Mazaheri et al., 2009;2013; Masiol and Harrison, 2014; Lobo et al., 2015) as well as from other anthropogenic (e.g., Schneider et al., 2005; Chen et al., 2011; Cheung et al., 2012; Stevens et al., 2012; Kumar et al., 2013;2014; Vu et al., 2015b) and natural (e.g., Kulmala et al., 1998; O'Dowd et al., 1998;1999; Kulmala and Kerminen, 2008; Riccobono et al., 2014) sources. This factor does not show any significant ( $p < 0.05$ ) and strong ( $r \geq |0.6|$ ) correlation with other measured species, but shows a weak ( $|0.4| \leq r < |0.6|$ ) correlation with Factor 2 (Table 2). Its diurnal variation (Figure 5) shows higher concentrations between 6 am and 10 pm, and well agrees with the airport flight movements (Figure 2). The polar plot analysis also indicates enhanced levels when winds  $> 2 \text{ m s}^{-1}$  blow from the airfield sectors (SW). All these insights are consistent with the location of Heathrow, i.e. the most plausible interpretation is related to the aircraft engine exhaust emissions. This interpretation is also supported by Keuken et al. (2015), which shows that the PNSD in an area affected by emissions from Schiphol airport (The Netherlands) is dominated by ultrafine (10-20 nm) particles. The large contribution of this factor to the total PNC is not surprising if compared to the results reported for the Los Angeles international airport by Hudda et al. (2014) (emissions from the airport increased PNC 4- to 5-fold at 8–10 km downwind the airfield). Since the airport of Los Angeles and LHR have comparable aircraft traffic, the quite high concentrations found in this study (on annual average nucleation particles are ~10 times higher than those measured in North Kensington urban

background by Vu et al. (2016)) are consistent with the sampling location chosen in this study (~1.2 km to the airfield). In addition, this result also agrees with previous studies on the impacts of LHR on local air quality; Carslaw et al. (2006) and Masiol and Harrison (2015) found comparable percent contributions of LHR emissions on NO<sub>2</sub> levels in the study area (approx. 25-30%). However, the lack of correlations with NO and NO<sub>2</sub> (tracers for aircraft emissions) is probably due to the presence of several other sources of nitrogen oxides in the area, such as the heavy traffic generated from the airport and from the nearby motorways.

*Factor 2* is made up of ultrafine particles in the nucleation-Aitken range (one main peak at 20-35 nm) and accounts for 28% (DISP 25-30%) of PNC; its contribution to the volume distribution is low (~2%) and peaks at 22-45 nm and at 140-220 nm (Figure 5; Table 1). Several insights seem to link this factor to road traffic emissions: (i) the modal structure; (ii) the strong association with morning and evening rush hours, and (iii) the significant increase for winds in the west and south-westerly sectors consistent with emissions generated from local busy roads close to LHR, Tunnel Rd. and M25 motorway. A similar mode in the nucleation range has been extensively attributed to the size distribution from road traffic (e.g., Vogt et al., 2003; Zhang et al., 2004; Ntziachristos et al., 2007; Vu et al., 2015b) and the growth of nucleation particles from diesel vehicles (Mayer and Ristovski, 2007; Wehner et al., 2009). For example, Charron and Harrison (2003) reported that particles in the range 30–60 nm show a stronger association with light-duty traffic at a traffic hotspot in central London (Marylebone Rd.); Janhäll et al. (2004) reported an average particle size distribution peaking at 15-30 nm during morning peak high traffic intensity in the city of Göteborg (Sweden), which has a car fleet comparable to the UK; Ntziachristos et al. (2007) found a sharp mode at 20-30 nm in sampling from engine exhausts. In addition, PMF factors with similar modal structures were found in other studies and were attributed to road traffic emissions: among others, Harrison et al. (2011) linked a factor peaking at 20 nm to primary road traffic emissions near a major UK highway; Masiol et al. (2016) measured PNSD in an international airport in Northern

Italy during summer and interpreted a factor with a clear mode at 35–40 nm as road traffic from the nearby city; Beddows et al. (2015) and Vu et al. (2016) found traffic factors with modal diameter at around 30 nm in an urban background site in London (North Kensington); Sowlat et al. (2016) reported a factor peaking at 20–40 nm in number concentration and at around 30–40 nm in volume concentration in Los Angeles (US) and interpreted it as traffic tailpipe emissions. However, this factor lacks significant positive correlations with primary road traffic tracers (nitrogen oxides, eBC; Table 2), while other studies have reported weak positive correlations with such species (Harrison et al., 2011; Masiol et al., 2016; Vu et al., 2016; Sowlat et al., 2016). Similarly to factor 1, this latter result may be due to the difference in the time resolution between chemical species and PNSD and the presence of several sources of nitrogen oxides in the area.

*Factor 3* is mostly represented by 25–90 nm particles and contributes about 19% (17–21%) to the total number concentration (Figure 5; Table 1). It also shows a second mode below the SMPS detection limit (14 nm), however, the DISP range clearly indicates that this part of the profile is affected by a large amount of rotational ambiguity, so that the presence of this second mode should be interpreted with caution. The volume concentration peaks at around 40–100 nm and 250–450 nm. The factor contribution is higher during rush hours, but the morning peak occurs 1 h later than in factor 2. The wind directionality shows increases for air masses blowing gently ( $<4 \text{ m s}^{-1}$ ) from W and for calm wind periods, suggesting a quite local source; however, also an increase of concentrations is found for higher wind regimes ( $>6 \text{ m s}^{-1}$ ) from the East (London). Factor 3 also shows significant positive correlations with NO (0.43) and NO<sub>2</sub> (0.61) (Table 2). All these insights seem to point to an aged road traffic source. This interpretation is also supported by Vu et al. (2016), who found a similar factor in London (North Kensington) peaking at ~20–100 nm. In this context, several source apportionment studies on PNSDs have attributed more than one factor to road traffic (e.g. Kasumba et al., 2009; Thimmaiah et al., 2009; Harrison et al., 2011; Liu et al., 2014; Al-Dabbous and Kumar, 2015; Vu et al., 2016; Sowlat et al., 2016). This result is not

surprising in areas where heavy traffic is widespread, as particles may undergo condensation, agglomeration, evaporation and dilution processes and, consequently, they may change modal characteristics in time and space. Such atmospheric processes are the main mechanisms reshaping PNSDs after primary exhaust is emitted into the atmosphere and have been discussed in several studies (Shi et al., 1999; Kim et al., 2004; Zhang et al., 2005; Zhou et al., 2005; Kulmala and Kerminen, 2008; Zhang et al., 2011; Harrison et al., 2016).

*Factor 4* is made up of particles over a wide range (50-200 nm with a clear mode at ~80 nm for PNC and 60-300 nm for PVC). The factor contributes 14% of PNC, but accounts for the main percentage of the volume concentration (33%). This factor correlates well with gaseous pollutants linked to combustion sources (mostly road traffic), i.e. NO (0.6), NO<sub>2</sub> (0.76), and non-volatile primary pollutants, such as eBC (0.62), NVPM<sub>2.5</sub> (0.62) and EC (0.75) (Table 2). The factor also strongly correlates with OC (0.84) and sulphate (0.75). The diurnal pattern shows two main peaks in the morning and evening rush hours (Figure 5), but the concentrations recorded between the two maxima are higher overnight than during daytime. This pattern suggests that both local emission sources and the dynamics of the mixing layer may play a key role in shaping its diurnal cycle, i.e. emitted pollutants undergo a wide dispersion within the expanded mixing layer during the daytime, while the drop of the mixing layer top occurring overnight restricts those pollutants to a layer close to ground level. The polar plot indicates increased levels for calm wind conditions or winds blowing from London (East sectors); in addition, the factor is strongly negatively correlated with wind speed (-0.64) (Table 2).

All these insights suggest that Factor 4 represents the fingerprint of the London pollution. Several studies carried out in London (Beddows et al., 2009;2015; Vu et al., 2016) and other megacities (e.g., New York: Masiol et al., 2017) have reported similar results, all interpreting this source profile as urban background (or urban accumulation mode). This source comprises both the solid



621 particle mode from traffic emissions (Harrison et al., 2011; Pant and Harrison, 2013; Dall'Osto et  
622 al., 2012) and secondary species condensed upon pre-existing particles acting as condensation  
623 nuclei, including secondary sulphate, nitrate and organic aerosols. Secondary sulphate is formed  
624 through the atmospheric processing of local or distant SO<sub>2</sub> emissions (Kerminen et al., 2000) and  
625 neutralisation with ammonia (Benson et al., 2011). Nitrate aerosol is formed through the oxidation  
626 of NO<sub>2</sub> to nitrate and the consequent neutralization with ammonia (Seinfeld and Pandis, 2006) and  
627 occurs during both daytime and night-time; however the semivolatile nature of ammonium nitrate,  
628 makes its partitioning to the condensed-phase very weak. This behaviour also favours the  
629 occurrence of negative artefacts in filter-based sampling, which may explain the lack of significant  
630 correlations between the factor and the PM<sub>2.5</sub>-bound nitrate (Table 2). On the contrary, the increase  
631 of the intensity of factor 4 during the night-time and the significant association with NO<sub>2</sub> are highly  
632 consistent with the chemistry driving the heterogeneous reactions of N<sub>2</sub>O<sub>5</sub> and NO<sub>3</sub> on aerosol  
633 surfaces (Bertram and Thornton, 2009; Brown and Stutz, 2012). In view of this, Dall'Osto et al.  
634 (2009) reported that most nitrate particles in London are: (i) locally produced in urban locations  
635 during nighttime; (ii) mainly present in particles smaller than 300 nm and (iii) internally mixed with  
636 sulphate, ammonium, EC and OC.

637

638 Factors 5 and 6 make small contributions to PNC (4-7% and 1-4%, respectively), but are relevant  
639 for the volume concentration (37% and 21%, respectively). Factor 5 shows a main accumulation  
640 mode in number concentration at 110-250 nm and two more modes at ~30-70 nm and below 14 nm  
641 (Figure 5; Table 1); however, the latter two modes suffer of large rotational ambiguity and should  
642 be interpreted with care. On the contrary, it exhibits a wide mode in volume concentration ranging  
643 from ~100 to ~500 nm. Factor 6 has two relevant modes in number concentration at 55-120 nm and  
644 230-400 nm, and two modes in volume concentration at 260-500 nm and 75-140 nm.

645

646 These factors still present two peaks corresponding to the rush hours, but the morning peak occurs  
647 1-2 h earlier than in the road traffic-related factors, i.e. when ambient temperature reaches its daily  
648 minimum. Both factors correlate well with secondary aerosol tracers (nitrate, sulphate, OC) and  
649 non-volatile components (eBC, EC, NVPM<sub>2.5</sub>), but Factor 6 exhibits much higher correlation  
650 coefficients (Table 2). Despite the polar plots indicating the main wind directionality toward N-E  
651 sectors, the analysis of air mass histories through the CWT model (Figure 7) clearly indicates likely  
652 continental origin areas rather than local sources.

653

654 Vu et al. (2016) observed two factors in North Kensington with very similar modal structures, daily  
655 patterns, correlations with PM<sub>2.5</sub>-bound species and external source areas maps. Therefore, their  
656 interpretation is confirmed also in this study, i.e. mixed secondary aerosol (Factor 5) and inorganic  
657 secondary aerosol (Factor 6). Both factors are clearly originated from continental Europe and are  
658 consistent with a previous receptor modelling study carried out in a rural background site  
659 representative of the southern UK (Charron et al., 2013). Similar origin and formation mechanisms  
660 also explain their strong correlation (0.75). Although it is not reasonable to extract much more  
661 information from these data due to the short period of sampling and the large uncertainty associated  
662 with back-trajectory analysis, it can be observed that Factor 5 shows a wide source area all over  
663 Central Europe, while Factor 6 exhibits two distinct hotspots (Central and North-eastern Europe).

664

665

### 666 3.3.2 Cold season

667 The 6 factors identified during the cold period (Figure 6) are similar to those for the warm season.  
668 *Factor 1* is composed of a high proportion of particles in the nucleation range with a sharp mode at  
669 ~15 nm. It accounts for 33% (32-35%) of PNC and less than 2% of PVC. The polar plot reveals  
670 increased concentrations for moderate winds blowing from the airport sector and the diurnal pattern  
671 is also compatible with the aircraft traffic. No statistically significant correlations are found with

any other monitored species (Table 3). Therefore, Factor 1 may be attributed to the airport emissions related to aircraft engine exhaust. As in the warm season, factor 1 is moderately correlated with factor 2 (fresh road traffic,  $r=0.55$ ), indicating a quite clear relationship between the two sources.

*Factor 2* represents particles in the 15-35 nm range of number concentration, accounting for 35% (33-37%) of total PNC (Figure 6; Table 1). Its importance for volume concentration is minimal (3%) with two modes at 30 and 200 nm. The diurnal pattern and the wind directionality are compatible with LHR as a source and it shows a weak positive correlation with  $\text{NO}_2$  (0.42) and a strong correlation with nitrate (0.63) (Table 3). Despite its similarity and relationship with Factor 1 and the consequent similar potential origin, Factor 2 may represent a different source: Factors 1 and 2 remain clearly separated even at solutions down to 4 factors, demonstrating their structural robustness and the lack of potential artefacts affecting the PMF solution. Consequently, it can be concluded that they do not represent over-resolved solutions (i.e. factor splitting). The most plausible interpretation for Factor 2 is therefore the same as for the warm season, i.e. fresh road traffic emissions. Furthermore, this factor can be attributed to the road traffic generated by the airport and nearby major roads.

*Factor 3* includes most of the particles in the Aitken range and accounts for 19% (18-20%) of PNC. Its contribution to particle volume concentration is relevant (9%) with a main peak at around 100 nm and a secondary peak at 400 nm (Table 1). It presents two rush hours peaks and the polar plot reveals an origin from the SW quadrant. However, as with the warm period, the wind directionality suggests increases for slower wind regimes than the fresh road traffic factor and for more westerly sectors, which are not compatible with the airfield location. Since factor 3 correlates well (Table 3) with a number of other pollutants linked to primary emissions from road traffic ( $\text{NO}$  (0.51),  $\text{NO}_2$

697 (0.81), eBC (0.52), PM<sub>2.5</sub> (0.53), OC (0.79) and EC (0.83)), it represents a second road traffic  
698 factor, more affected by aging in the atmosphere than factor 2.  
699

700 Despite the wind regimes from NE sectors being poorly represented during the cold campaign,  
701 *Factor 4* is the only one showing a possible origin from London and for calm wind periods. As with  
702 the warm season, it is composed of a wide range of particles encompassing the Aitken and  
703 accumulation modes (50 to 150 nm), while the peak in volume concentration is at 170 nm (Table 1).  
704 The diurnal pattern (Figure 6) is clearly related to the mixing layer dynamics and the correlation  
705 analysis reveals strong relationships with many species (NO, NO<sub>2</sub>, eBC, Delta-C, NVPM<sub>2.5</sub>, OC,  
706 EC, nitrate, ammonium and potassium; Table 3). Consequently, it is concluded that it represents the  
707 urban accumulation mode, whose contribution to the total volume concentration is also similar to  
708 the warm season (33%). It is interesting to note the large similarity with the urban accumulation  
709 mode found in the warm season, from which it differs slightly only in the diurnal pattern (higher  
710 overnight) and in the presence of a strong correlation with nitrate ( $r=0.88$ ), possibly due to the  
711 lesser extent of negative artefacts on PM<sub>2.5</sub> filter samples.  
712

713 The last two factors are interpreted as due to secondary aerosols. Their modal structures, their  
714 contributions to total PNC and PVC, and their correlations with PM<sub>2.5</sub>-bound species (Table 3;  
715 Figure 6) largely reflect the results obtained for the warm period. However, the CWT maps (Figure  
716 7) highlight different source areas, i.e. the origin of the secondary aerosols is regional (UK and  
717 Northern Europe). In addition, the presence of strong positive correlations with chloride may also  
718 indicate a contribution from the transport of sea-salt aerosol.  
719

720 **3.3 Comparison of *k*-means and PMF**

721 The cluster analysis revealed the presence of 5 characteristic PNSD shapes during both the seasons.  
722 These spectra have been linked to potential sources in the study area, i.e. road traffic, airport

723 activities, and secondary aerosol formation processes. However, the cluster analysis is mostly  
724 driven by the spectral size regions with higher particle number concentrations, i.e. it has the  
725 disadvantage of partitioning the single observations predominantly according to the finest region of  
726 the size distribution. This limitation is well illustrated by the poor (almost null) separation of  
727 clusters based on the particle volume distributions (all clusters showed quite similar particle volume  
728 spectra). In addition, cluster analysis also has the disadvantage of linking each cluster to a single  
729 source and does not easily account for PNSD resulting from the mix of two or more different  
730 sources.

731

732 In contrast, the PMF analysis computed over the PNSD also accounts well for the sources with a  
733 small impact on the number distribution, but having a larger influence on the particle volume size  
734 distributions and, therefore, on the particle mass concentration. Despite the differences in the two  
735 methods, some further information can be extracted by combining the results of cluster and PMF  
736 analysis. Figure 8 shows the statistics of normalised PMF source contributions relating to each  
737 single cluster.

738

739 For the warm period, significantly higher (0.05 significance) PMF contributions of the airport factor  
740 (F1) are measured for cluster 1 (average normalised contribution  $\sim 3.5$ ). This result indicates that the  
741 airport fingerprint was well captured by both source apportionment methods. During the cold  
742 season, the airport factor (F1) is significantly higher for both clusters 1 and 5 (average normalised  
743 contributions of  $\sim 2$  and  $\sim 3$ , respectively). While cluster 5 presents significant high PMF  
744 contributions only for factor 1, cluster 1 also shows high contributions of factor 2 (fresh road  
745 traffic). This result indicates that cluster 5 may be linked as the typical PNSD spectra for airport  
746 emissions, while cluster 2 likely represents mixed emissions from aircraft and airport-related traffic.  
747 A close analysis of wind roses for the two clusters in the cold season (Figure 4) reveals that cluster  
748 5 occurs at significantly higher wind speed regimes than cluster 1 (Mann-Whitney-Wilcoxon test at

0.05 significance level), i.e. average wind speeds of 8.3 and 5.9 m s<sup>-1</sup>, respectively. As a consequence, the different wind regimes may well be responsible for the split between the two clusters.

Results for fresh traffic emissions also agree between the two methods. Factors 2 exhibit the higher normalised contributions to clusters 5 (normalised contribution 2.5) and 1 (normalised contribution ~3) for the warm and cold period, respectively (Figure 8). However, in winter it is evident that PNSDs grouped on cluster 1 are also strongly influenced by airport emissions, probably due to the lower mixing layer height and, thus, a lesser dispersion in the atmosphere.

Clusters 4 for both the periods show enrichments in the contributions for 4 PMF sources (aged road traffic, urban accumulation and the two secondary aerosols) (Figure 8). This further emphasises that cluster 4 represents the typical PNSD during daytime resulting from the mixing of different sources. In a similar way, clusters 3 and 2 in the warm and cold periods, respectively, represent the typical nighttime spectra (Figures 3 and 4), i.e. they exhibit similar partitioning over the PMF sources and similar daily cycles.

### **3.4 Analysis of a Large Regional Nucleation Event**

Regional photochemical nucleation episodes are regularly recorded in the Southern and Eastern UK. Their general characteristics have been reported in a number of studies (e.g., Alam et al., 2003; Charron et al., 2007; 2008; Beddows et al., 2015; Vu et al., 2016) and can be summarised as follows: (i) particle modality at around 20 nm; (ii) higher frequency around noon in association with the peak in actinic flux intensities; (iii) clear seasonal cycles (higher average contribution levels in the summer, from June to September); (iv) marked directionality from the westerly sectors, reflecting maritime atmospheric circulation regimes, with high wind speed and low PM<sub>2.5</sub> concentrations.

775 A strong regional nucleation event occurred during the warm period sampling campaign (starting on  
 776 7th September at 1 pm UTC and lasting for about 12 h). Increases of PNC were almost  
 777 simultaneously recorded at Harlington and at Harwell, a national network rural background site  
 778 located approx. 60 km WNW of LHR and representative of the regional background levels of air  
 779 pollution across the Southern UK. The comparison of PNC time series at the two sites is provided  
 780 as Figure SI10. Figure 9 shows the contour plots of SMPS data recorded at Harlington between 7th  
 781 and 8th September as well as the hourly averaged concentrations of nucleation, Aitken and  
 782 accumulation particles, TEOM-FDMS PM<sub>2.5</sub> mass and the contributions of Factors 1 to 4 extracted  
 783 by the PMF. Figure 9 also reports the hourly counts of number of clusters extracted by the *k*-means  
 784 analysis. The contour plot shows a typical “banana” shape with particle mode growing from ~20 nm  
 785 (1 pm) to ~100 nm (overnight). The episode strongly influenced the PNSDs until around midnight;  
 786 however its effect is also visible over the first half of 8th September. The time series (Figure 9)  
 787 exhibits a clear peak in nucleation particles between 1 pm and 3 pm followed by peaks of Aitken (3-  
 788 11 pm) and accumulation mode (8 pm-2 am) particles. The back-trajectory analysis (Figure SI11)  
 789 revealed that the event occurred when north-westerly fresh (and clean) maritime air masses were  
 790 advected from the Atlantic. This is also supported by the PM<sub>2.5</sub> mass, which exhibited a fast drop of  
 791 concentrations just a few hours before the event ( $-30 \mu\text{g m}^{-3}$  in 3 hours, i.e. from  $40 \mu\text{g m}^{-3}$  at 6 am  
 792 to  $10 \mu\text{g m}^{-3}$  at 9 am, Figure 9), probably reducing the condensation sink and facilitating nucleation.  
 793  
 794 Both atmospheric nucleation and aircraft engines are recognised to produce particles in the  
 795 nucleation range. The analysis of this single –but strong– episode gives insights into how much the  
 796 source apportionment results can potentially be affected by regional nucleation. This latter analysis  
 797 is possible because the wind directionality during the entire episode was from N sectors, i.e. the  
 798 contribution of LHR can be considered negligible.

799

800 The results of cluster analysis were affected by the event. Before the episode, the PNSD spectra  
801 were mostly categorised as clusters 3 and 4 (urban background and daytime pollution, respectively),  
802 i.e. the clusters mostly recorded under north-easterly wind regimes (Figure 3). About 50% and 30%  
803 of the clusters were then categorised as “airport” in the first and second hour of the episode,  
804 respectively (Figure 9). Since the wind directionality is inconsistent with an origin from the airfield,  
805 this categorisation is likely the result of the nucleation event. The growing of particles in the hours  
806 after the beginning of the event has further driven the cluster results: (i) about 60-80% of PNSDs  
807 were categorised as “fresh road traffic” (cluster 5) after 2-3 hours, and (ii) 80-100% of PNSDs were  
808 clustered as “nighttime regional pollution” (cluster 2) after 4-6 hours. In a similar way, PMF results  
809 were affected by the event (Figure 9), with a sharp increase of contribution levels for: (i) factor 1  
810 (airport) from  $1.5 \times 10^3$  particles  $\text{cm}^{-3}$  at noon to  $13.3 \times 10^3$  particles  $\text{cm}^{-3}$  at 2 pm; (ii) factor 2  
811 (fresh road traffic) from  $0.5 \times 10^3$  particles  $\text{cm}^{-3}$  at 1 pm to  $21 \times 10^3$  particles  $\text{cm}^{-3}$  at 3 pm; and (iii)  
812 factor 3 (aged road traffic) from  $2.1 \times 10^3$  particles  $\text{cm}^{-3}$  at 2 pm to approx.  $15 \times 10^3$  particles  $\text{cm}^{-3}$  at  
813 5-6 pm.

814

815 This episode was the main nucleation event recorded during the two sampling campaigns. Other  
816 possible episodes also occurred (mostly during the warm season), but they were much less  
817 significant and often hard to detect. This qualitative analysis points to some conclusions: (i)  
818 regional photochemical nucleation events may have an effect on clustering and PMF results; (ii) the  
819 effect may lead to an “additive” bias, mostly over the “airport” and “road traffic” factors and  
820 clusters; (iii) the effect of regional nucleation events in the study area is largely overwhelmed by the  
821 strength of local sources, but in other locations with more frequent nucleation events it may be more  
822 important to identify and separate them.

823

824

825



## 826 4 CONCLUSIONS

827 The effect of airport emissions upon the particle number concentration and size distribution was  
828 assessed at a site close to a major European airport (Heathrow) serving a megacity (London). The  
829 conclusions to be drawn are:

- 830 • High particle number concentrations were recorded for the finest sizes (nucleation <30 nm and  
831 Aitken nuclei 30-100 nm) if compared to an urban background site in London (N. Kensington).
- 832 • Polar plot analysis indicates that Heathrow is a strong potential source for NO<sub>2</sub>, nucleation and  
833 Aitken particles, but its contribution to the mass concentration of PM<sub>2.5</sub> and eBC is very small.  
834 On the contrary, the urban area of London appears to be the main source for PM and eBC.
- 835 • The *k*-means cluster analysis has revealed that 20% of PNSDs are mostly shaped by airport  
836 direct emissions, but particle size spectra are also strongly affected by other local sources  
837 (mostly fresh and aged road traffic during daytime) and the reduction of mixing layer depth  
838 (during nighttime). Typical PNSD spectra have been identified for nighttime and daytime  
839 pollution as well. Such spectra are likely the result of multiple source mixtures.
- 840 • PMF analysis revealed that the fingerprint of Heathrow has a peculiar modal structure peaking  
841 at <20 nm. The direct airport emissions account for 30-35% of total particles in both the  
842 seasons. Such results are in line with percent estimations for NO<sub>2</sub> reported in previous studies.
- 843 • Other major contributors to PNC are fresh (24-36%) and aged (16-21%) road traffic emissions.  
844 Despite both applied source apportionment methods failing to fully disaggregate the emissions  
845 from the local traffic (including motorway) and traffic generated by the airport, results suggest  
846 that road traffic sources may contribute to the total PNC more than Heathrow (40-56%).  
847 However, making a clear distinction between the influence of traffic generated by the airport  
848 from other road traffic is not feasible from this analysis.
- 849 • An urban accumulation mode was found. This source presents a wide mode between 50-150  
850 nm and accounts for around 10% of PNC. The wind directionality is consistent with the  
851 advection of air masses from London. It is more evident overnight due to the drop of the

852 mixing layer top, the subsequent increase in air pollutants at ground level and the generation of  
853 nighttime secondary nitrate aerosols.

854 • Secondary sources accounted for less than 6% in number concentrations but for more than 50%  
855 in volume concentration. Long-range transport has a key role in advecting polluted air masses  
856 from mainland Europe.

## 858 **ACKNOWLEDGEMENTS**

859 The authors gratefully acknowledge: (i) the European Union for funding the Marie Curie Intra-  
860 European Fellowship for career development to M. Masiol through the project ‘CHEERS’  
861 (Chemical and Physical Properties and Source Apportionment of Airport Emissions in the context  
862 of European Air Quality Directives, call: FP7-PEOPLE-2012-IEF, project no. 328542); (ii) the  
863 Natural Environment Research Council for support of D. Beddows under award  
864 R8/H12/83/2017/18; (iii) Heathrow Airport Ltd and Ricardo-AEA for supplying aircraft movement  
865 data and for the valuable exchange of information and discussion, in particular Katherine Rolfe,  
866 Elizabeth Hegarty (Heathrow), Brian Stacey (Ricardo-AEA) and David Vowles; (iv) DEFRA  
867 Automatic Urban and Rural Network, and London Air Quality Network for providing pollutant  
868 data; (v) Met Office and BADC for weather data; (vi) the NOAA Air Resources Laboratory (ARL)  
869 for the provision of the HYSPLIT transport and dispersion model used in this publication; (vii) the  
870 UK Department for Transport, Road Traffic and Road Freight Statistics, for providing M4 and M25  
871 traffic data; and (viii) Dr. Stefania Squizzato (University of Rochester, NY, USA) for the valuable  
872 exchange of information.

## 875 REFERENCES

- 876 ACI (Airport Council International): ACI releases preliminary world airport traffic rankings.  
 877 Airports Council International, Montreal. Available at: [http://www.aci.aero/News/Releases/Most-](http://www.aci.aero/News/Releases/Most-Recent/2016/04/04/ACI-releases-preliminary-world-airport-traffic-rankings-)  
 878 Recent/2016/04/04/ACI-releases-preliminary-world-airport-traffic-rankings- [last accessed: June  
 879 2016].  
 880  
 881 AEA: Heathrow Airport Air Quality Modelling for 2008/9: Results and Model Evaluation. Report  
 882 by AEA Energy & Environment on behalf of BAA, July 2010. AEAT/ENV/R/2948/Issue 1.  
 883  
 884 Al-Dabbous, A. N., Kumar, P.: Source apportionment of airborne nanoparticles in a Middle Eastern  
 885 city using positive matrix factorization, *Environ. Sci. Process Impacts*, 17, 802-812, 2015.  
 886  
 887 Alam, A., Shi, J. P. and Harrison, R. M.: Observations of new particle formation in urban air, *J.*  
 888 *Geophys. Res.*, 108, 4093-4107, 2003. doi:10.1029/2001JD001417  
 889  
 890 Anderson, B. E., Branham, H.-S., Hudgins, C. H., Plant, J. V., Ballenthin, J. O., Miller, T. M.,  
 891 Viggiano, A. A., Blake, D. R., Boudries, H., Canagaratna, M., Miake-Lye, R. C., Onasch, T.,  
 892 Wormhoudt, J., Worsnop, D., Brunke, K. E., Culler, S., Penko P., Sanders, T., Han, H.-S., Lee, P.,  
 893 Pui, D. Y. H., Thornhill, K. L., Winstead, E. L.: Experiment to Characterize Aircraft Volatile  
 894 Aerosol and Trace-Species Emissions (EXCAVATE), NASA/TM-2005-213783, National  
 895 Aeronautics and Space Administration, Hampton, VA., 2005.  
 896  
 897 Anttila, P., Tuovinen, J. P., Niemi, J. V.: Primary NO<sub>2</sub> emissions and their role in the development  
 898 of NO<sub>2</sub> concentrations in a traffic environment, *Atmos. Environ.*, 45, 986-992, 2011.  
 899  
 900 Atkinson, R. W., Fuller, G. W., Anderson, H. R., Harrison, R. M., Armstrong, B.: Urban ambient  
 901 particle metrics and health: a time-series analysis, *Epidemiol.*, 21, 501-511, 2010.  
 902  
 903 Beddows, D. C. S., Dall'Osto, M., Harrison, R. M.: Cluster analysis of rural, urban and curbside  
 904 atmospheric particle size data, *Environ. Sci. Technol.*, 43, 4694-4700, 2009.  
 905  
 906 Beddows, D. C. S., Dall'Osto, M., Harrison, R. M., Kulmala, M., Asmi, A., Wiedensohler, A., Laj,  
 907 P., Fjaeraa, A. M., Sellegri, K., Birmili, W., Bukowiecki, N., Weingartner, E., Baltensperger, U.,  
 908 Zdimal, V., Zikova, N., Putaud, J.-P., Marinoni, A., Tunved, P., Hansson, H.-C., Fiebig, M.,  
 909 Kivekäs, N., Swietlicki, E., Lihavainen, H., Asmi, E., Ulevicius, V., Aalto, P. P., Mihalopoulos, N.,  
 910 Kalivitis, N., Kalapov, I., Kiss, G., de Leeuw, G., Henzing, B., O'Dowd, C., Jennings, S. G., Flentje,  
 911 H., Meinhardt, F., Ries, L., Denier van der Gon, H. A. C., Visschedijk, A. J. H.: Variations in  
 912 tropospheric submicron particle size distributions across the European continent 2008-2009,  
 913 *Atmos. Chem. Phys.*, 14, 4327-4348, 2014.  
 914  
 915 Beddows D. C. S., Harrison R. M., Green D. C. and Fuller G. W.: Receptor modelling of both  
 916 particle composition and size distribution from a background site in London, UK., *Atmos. Chem.*  
 917 *Phys.*, 15, 10107-10125, 2015.  
 918  
 919 Belis, C. A., Larsen, B. R., Amato, F., El Haddad, I., Favez, O., Harrison, R. M., Hopke, P. K.,  
 920 Nava, S., Paatero, P., Prévôt, A., Quass, U., Vecchi, R. and Viana, M.: European guide on air  
 921 pollution source apportionment with receptor models, JRC Reference Reports EUR26080 EN,  
 922 2014.  
 923

924 Benson, D. R., Yu, J. H., Markovich, A., Lee, S.-H.: Ternary homogeneous nucleation of H<sub>2</sub>SO<sub>4</sub>,  
 925 NH<sub>3</sub>, and H<sub>2</sub>O under conditions relevant to the lower troposphere, *Atmos. Chem. Phys.*, 11, 4755-  
 926 4766, 2011.

927 Bertram, T. H. and Thornton, J. A.: Toward a general parameterization of N<sub>2</sub>O<sub>5</sub> reactivity on  
 928 aqueous particles: the competing effects of particle liquid water, nitrate and chloride, *Atmos. Chem.*  
 929 *Phys.*, 9, 8351-8363, 2009.

930

931 Bigi A and Harrison R. M.: Analysis of the air pollution climate at a central urban background site,  
 932 *Atmos. Environ.*, 44, 2004-2012, 2010.

933

934 Brines, M., Dall'Osto, M., Beddows, D. C. S., Harrison, R. M. and Querol, X.: Simplifying aerosol  
 935 size distributions modes simultaneously detected at four monitoring sites during SAPUSS, *Atmos.*  
 936 *Chem. Phys.*, 14, 2973-2986, 2014.

937

938 Brines, M., Dall'Osto, M., Beddows, D., Harrison, R., Gómez-Moreno, F., Núñez, L., Artíñano, B.,  
 939 Costabile, F., Gobbi, G. And Salimi, F.: Traffic and nucleation events as main sources of ultrafine  
 940 particles in high-insolation developed world cities, *Atmos. Chem. Phys.*, 15, 5929-5945, 2015.

941

942 Brown, S. S. and Stutz, J.: Nighttime radical observations and chemistry, *Chem. Soc. Rev.*, 41,  
 943 6405-6447, 2012.

944

945 Brown, S. G., Eberly, S., Paatero, P. and Norris, G. A.: Methods for estimating uncertainty in PMF  
 946 solutions: Examples with ambient air and water quality data and guidance on reporting PMF results,  
 947 *Sci.Total Environ.*, 518, 626-635, 2015.

948

949 Carslaw, D. C. and Ropkins, K.: Openair - an R package for air quality data analysis, *Environ.*  
 950 *Model. Softw.*, 27-28, 52-61, 2012.

951

952 Carslaw, D. C., Beevers, S. D., Ropkins, K. and Bell, M. C.: Detecting and quantifying aircraft and  
 953 other on-airport contributions to ambient nitrogen oxides in the vicinity of a large international  
 954 airport, *Atmos. Environ.*, 40, 5424-5434, 2006.

955

956 Carslaw, D. C., Beevers, S. D. and Bell, M. C.: Risks of exceeding the hourly EU limit value for  
 957 nitrogen dioxide resulting from increased road transport emissions of primary nitrogen dioxide,  
 958 *Atmos. Environ.*, 41, 2073-2082, 2007.

959

960 Chandrasekaran, S. R., Hopke, P. K., Newtown, M. and Hurlbut, A.: Residential-scale biomass  
 961 boiler emissions and efficiency characterization for several fuels, *Energy & Fuels*, 27, 4840-4849,  
 962 2013.

963

964 Charron, A. and Harrison, R. M.: Primary particle formation from vehicle emissions during exhaust  
 965 dilution in the roadside atmosphere, *Atmos. Environ.*, 37, 4109-4119, 2003.

966

967 Charron, A., Degrendele, C., Laongsri, B. and Harrison, R. M.: Receptor modelling of secondary  
 968 and carbonaceous particulate matter at a southern UK site, *Atmos. Chem. Phys.* 13, 1879-1894,  
 969 2013.

970

971 Charron, A., Birmili, W. and Harrison, R. M.: Factors influencing new particle formation at the rural  
 972 site, Harwell, United Kingdom, *J. Geophys. Res.*, 112, D14210, 2007. doi:10.1029/2007JD008425.

973

974

975 Charron, A., Birmili, W. and Harrison, R. M.: Fingerprinting particle origins according to their size  
 976 distribution at a UK rural site, *J. Geophys. Res.*, 113, D07202, 2008. doi:10.1029/2007JD008562.  
 977

978 Chen, J. P., Tsai, T. S. and Liu, S. C.: Aerosol nucleation spikes in the planetary boundary layer,  
 979 *Atmos. Chem. Phys.*, 11, 7171-7184, 2011.  
 980

981 Cheung, H. C., Morawska, L., Ristovski, Z. D., and Wainwright, D.: Influence of medium range  
 982 transport of particles from nucleation burst on particle number concentration within the urban  
 983 airshed, *Atmos. Chem. Phys.*, 12, 4951-4962, 2012.  
 984

985 Clapp, L. J. and Jenkin, M. E.: Analysis of the relationship between ambient levels of O<sub>3</sub>, NO<sub>2</sub> and  
 986 NO as a function of NO<sub>x</sub> in the UK, *Atmos. Environ.*, 35, 6391-6405, 2001.  
 987

988 Costabile, F., Birmili, W., Klose, S., Tuch, T., Wehner, B., Wiedensohler, A., Franck, U.,  
 989 König, K. and Sonntag, A.: Spatio-temporal variability and principal components of the particle  
 990 number size distribution in an urban atmosphere, *Atmos. Chem. Phys.*, 9, 3163-3195, 2009.  
 991

992 Cyrys, J., Eeftens, M., Heinrich, J., Ampe, C., Armengaud, A., Beelen, R., Bellander, T.,  
 993 Beregszaszi, T., Birk, M., Cesaroni, G., Cirach, M., de Hoogh, K., De Nazelle, A., de Vocht, F.,  
 994 Declercq C., Dedele, A., Dimakopoulou, K., Eriksen, K., Galassi, C., Grauleviciene, R., Grivas, G.,  
 995 Gruzjeva, O., Hagenbjörk Gustafsson, A., Hoffmann, B., Iakovides, M., Ineichen, A., Krämer, U.,  
 996 Lanki, T., Lozano, P., Madsen, C., Meliefste, K., Modig, L., Mölterm, A., Mosler, G.,  
 997 Nieuwenhuijsen, M., Nonnemacher, M., Oldenwening, M., Peters, A., Pontet, S., Probst-Hensch,  
 998 N., Quass, U., Raaschou-Nielsen, O., Ranzi, A., Sugiri, D., Stephanou, E.G., Taimisto, P., Tsai, M.-  
 999 Y., Vaskövi, E., Villani, S., Wang, M., Brunekreef, B. and Hoek, G.: Variation of NO<sub>2</sub> and NO<sub>x</sub>  
 1000 concentrations between and within 36 European study areas: Results from the ESCAPE study,  
 1001 *Atmos. Environ.*, 62, 374-390, 2012.  
 1002

1003 Dall'Osto, M., Harrison, R. M., Coe, H., Williams, P. I. and Allan, J.D.: Real time chemical  
 1004 characterization of local and regional nitrate aerosols, *Atmos. Chem. Phys.*, 9, 3709-3720, 2009.  
 1005

1006 Dall'Osto, M., Thorpe, A., Beddows, D. C. S., Harrison, R. M., Barlow, J. F., Dunbar, T., Williams,  
 1007 P.I. and Coe, H.: Remarkable dynamics of nanoparticles in the urban atmosphere, *Atmos. Chem.*  
 1008 *Phys.*, 11, 6623-6637, 2011.  
 1009

1010 Dall'Osto, M., Beddows, D. C. S., Pey, J., Rodriguez, S., Alastuey, A., Harrison, R. M. and Querol,  
 1011 X.: Urban aerosol size distributions over the Mediterranean city of Barcelona, NE Spain, *Atmos.*  
 1012 *Chem. Phys.*, 12, 10693-10707, 2012.  
 1013

1014 DEFRA: Air Pollution in the UK 2015. UK Department for Environment, Food and Rural Affairs.  
 1015 Issue of September 2016. Available at: [https://uk-](https://uk-air.defra.gov.uk/assets/documents/annualreport/air_pollution_uk_2015_issue_1.pdf)  
 1016 [air.defra.gov.uk/assets/documents/annualreport/air\\_pollution\\_uk\\_2015\\_issue\\_1.pdf](https://uk-air.defra.gov.uk/assets/documents/annualreport/air_pollution_uk_2015_issue_1.pdf) (last accessed:  
 1017 November 2016).  
 1018

1019 Dodson, R. E., Houseman, E. A., Morin, B. and Levy, J. I.: An analysis of continuous black carbon  
 1020 concentrations in proximity to an airport and major roadways, *Atmos. Environ.*, 43, 3764-3773,  
 1021 2009.  
 1022

1023 Farias, F. and ApSimon, H.: Relative contributions from traffic and aircraft NO<sub>x</sub> emissions to  
 1024 exposure in West London, *Environ. Modell. Softw.*, 21, 477-485, 2006.  
 1025

1026 Finlayson-Pitts, B. J. and Pitts Jr, J. N.: Chemistry of the upper and lower atmosphere: theory,  
 1027 experiments, and applications. Academic press, 2000.  
 1028

1029 Grice, S., Stedman, J., Kent, A., Hobson, M., Norris, J., Abbott, J., Cooke S.: Recent trends and  
 1030 projections of primary NO<sub>2</sub> emissions in Europe, *Atmos. Environ.*, 43, 2154-2167, 2009.  
 1031

1032 Harrison, R. M., Beddows, D. C. S. and Dall'Osto, M.: PMF Analysis of wide-range particle size  
 1033 spectra collected on a major highway, *Environ. Sci. Technol.*, 45, 5522-5528, 2011.  
 1034

1035 Harrison, R.M., Dall'Osto, M., Beddows, D.C.S., Thorpe, A.J., Bloss, W.J., Allan, J.D., Coe, H.,  
 1036 Dorsey, J.R., Gallagher, M., Martin, C. and Whitehead, J.: Atmospheric chemistry and physics in  
 1037 the atmosphere of a developed megacity (London): an overview of the REPARTEE experiment and  
 1038 its conclusions. *Atmos. Chem. Phys.*, 12(6), 3065-3114, 2012.  
 1039

1040 Harrison, R. M., Beddows, D. C., Jones, A. M., Calvo, A., Alves, C. and Pio, C.: An evaluation of  
 1041 some issues regarding the use of aethalometers to measure woodsmoke concentrations, *Atmos.*  
 1042 *Environ.*, 80, 540-548, 2013.  
 1043

1044 Harrison, R. M., Jones, A. M., Beddows, D. C. S., Dall'Osto, M. and Nikolova, I.: Evaporation of  
 1045 traffic-generated nanoparticles during advection from source, *Atmos. Environ.*, 125, 1-7, 2016.  
 1046

1047 Herndon, S. C., Jayne, J. T., Lobo, P., Onasch, T. B., Fleming, G., Hagen, D. E., Whitefield, P. D.  
 1048 and Miake-Lye, R. C.: Commercial aircraft engine emissions characterization of in-use aircraft at  
 1049 Hartsfield-Jackson Atlanta International Airport, *Environ. Sci. Technol.*, 42, 1877-1883, 2008.  
 1050

1051 Hopke, P. K.: Review of receptor modeling methods for source apportionment. *JAWMA*, 66, 237-  
 1052 259, 2016.  
 1053

1054 Hsu, H.H., Adamkiewicz, G., Houseman, E.A., Vallarino, J., Melly, S.J., Wayson, R.L., Spengler,  
 1055 J.D. and Levy, J.I.: The relationship between aviation activities and ultrafine particulate matter  
 1056 concentrations near a mid-sized airport, *Atmos. Environ.*, 50, 328-337, 2012a.  
 1057

1058 Hsu, H.H., Adamkiewicz, G., Houseman, E.A., Vallarino, J., Melly, S.J., Wayson, R.L., Spengler,  
 1059 J.D. and Levy, J.I.: The relationship between aviation activities and ultrafine particulate matter  
 1060 concentrations near a mid-sized airport, *Atmos. Environ.*, 50, 328-337, 2012b.  
 1061

1062 Hsu, H. H., Adamkiewicz, G., Houseman, E. A., Zarubiak, D., Spengler, J. D. and Levy, J. I.:  
 1063 Contributions of aircraft arrivals and departures to ultrafine particle counts near Los Angeles  
 1064 International Airport, *Sci. Tot. Environ.*, 444, 347-355, 2013.  
 1065

1066 Hsu, H. H., Adamkiewicz, G., Houseman, E. A., Spengler, J. D., Levy and J.I.: Using mobile  
 1067 monitoring to characterize roadway and aircraft contributions to ultrafine particle concentrations  
 1068 near a mid-sized airport, *Atmos. Environ.*, 89, 688-695, 2014.  
 1069

1070 Hu, S., Fruin, S., Kozawa, K., Mara, S., Winer, A.M. and Paulson, S.E.: Aircraft emission impacts  
 1071 in a neighborhood adjacent to a general aviation airport in Southern California, *Environ. Sci.*  
 1072 *Technol.*, 43(21), 8039-8045, 2009.  
 1073

1074 Hudda, N., Gould, T., Hartin, K., Larson, T. V. and Fruin, S. A.: Emissions from an international  
 1075 airport increase particle number concentrations 4-fold at 10 km downwind, *Environ. Sci. Technol.*,  
 1076 48, 6628-6635, 2014.  
 1077

1078 Hudda, N., Simon, M. C., Zamore, W., Brugge, D. And Durant, J. L.: Aviation emissions impact  
 1079 ambient ultrafine particle concentrations in the greater Boston area, *Environ.Sci. Technol.*, 50,  
 1080 8514-8521, 2016.  
 1081  
 1082 Hudda, N., Fruin, S.A.: International airport impacts to air quality: size and related properties of  
 1083 large increases in ultrafine particle number concentrations, *Environ. Sci. Technol.*, 50, 3362-3370,  
 1084 2016.  
 1085  
 1086 Hussein, T., Molgaard, B., Hannuniemi, H., Martikainen, J., Jarvi, L., Wegner, T., Ripamonti, G.,  
 1087 Weber, S., Vesala, T. and Hameri, K.: Fingerprints of the urban particle number size distribution in  
 1088 Helsinki, Finland: local vs. regional characteristics, *Boreal Env. Res.*, 19, 1-20, 2014.  
 1089  
 1090 ICAO (International Civil Aviation Organization), Annual Report of the ICAO Council: 2014. The  
 1091 World of Air Transport in 2014, Appendix 1: [https://www.icao.int/annual-report-](https://www.icao.int/annual-report-2014/Documents/Appendix_1_en.pdf)  
 1092 [2014/Documents/Appendix\\_1\\_en.pdf](https://www.icao.int/annual-report-2014/Documents/Appendix_1_en.pdf), last access: 20 June 2017.  
 1093  
 1094 Janhäll S., Jonsson Å. M., Molnár P., Svensson E. A. and Hallquist M.: Size resolved traffic  
 1095 emission factors of submicrometer particles, *Atmos. Environ.*, 38, 4331-4340, 2004.  
 1096  
 1097 Jones, A.M., Harrison, R.M., Barratt, B. and Fuller, G.: A large reduction in airborne particle  
 1098 number concentrations at the time of the introduction of “sulphur free” diesel and the London Low  
 1099 Emission Zone, *Atmos. Environ.*, 50, 129-138, 2012.  
 1100  
 1101 Kasumba, J., Hopke, P. K., Chalupa, D. C. and Utell, M. J.: Comparison of sources of submicron  
 1102 particle number concentrations measured at two sites in Rochester, NY, *Sci. Total Environ.*, 407,  
 1103 5071-5084, 2009.  
 1104  
 1105 Kelly, F. J. and Fussell, J. C.: Size, source and chemical composition as determinants of toxicity  
 1106 attributable to ambient particulate matter, *Atmos. Environ.*, 60, 504-526, 2012.  
 1107 Kerminen, V. M., Pirjola, L., Boy, M., Eskola, A., Teinilä, K., Laakso, L., Asmi, A., Hienola, J.,  
 1108 Lauri, A., Vainio, V. And Lehtinen, K.: Interaction between SO<sub>2</sub> and submicron atmospheric  
 1109 particles, *Atmos. Res.*, 54, 41-57, 2000.  
 1110  
 1111 Keuken, M. P., Moerman, M., Zandveld, P., Henzing, J. S. and Hoek, G.: Total and size-resolved  
 1112 particle number and black carbon concentrations in urban areas near Schiphol airport (the  
 1113 Netherlands), *Atmos. Environ.*, 104 132-142, 2015.  
 1114  
 1115 Kim, E., Hopke, P. K., Larson, T. V. and Covert, D. S.: Analysis of ambient particle size  
 1116 distributions using unmix and positive matrix factorization, *Environ. Sci. Technol.*, 38, 202-209,  
 1117 2004.  
 1118  
 1119 Kinsey, J. S., Dong, Y., Williams, D. C. and Logan, R.: Physical characterization of the fine  
 1120 particle emissions from commercial aircraft engines during the aircraft particle emissions  
 1121 experiment (APEX) 1 to 3, *Atmos. Environ.*, 44, 2147-2156, 2010.  
 1122  
 1123 Klapmeyer, M.E. and Marr, L.C.: CO<sub>2</sub>, NO<sub>x</sub>, and Particle Emissions from Aircraft and Support  
 1124 Activities at a Regional Airport, *Environ. Sci. Technol.*, 46(20), 10974-10981, 2012.  
 1125  
 1126 Kley, D., Kleinmann, M., Sanderman, H. and Krupa, S.: Photochemical oxidants: state of the  
 1127 science, *Environ. Pollut.*, 100, 19-42, 1999.  
 1128

Knibbs, L. D., Cole-Hunter, T. and Morawska, L.: A review of commuter exposure to ultrafine particles and its health effects, *Atmos. Environ.*, 45, 2611-2622, 2011.

Kruskal, W.H. and Wallis, W.A., Use of ranks in one-criterion variance analysis. *J. Amer. Statist. Assoc.*, 47, 583-621, 1952.

Kulmala, M., Toivonen, A., Mäkelä, J. M. and Laaksonen, A.: Analysis of the growth of nucleation mode particles observed in Boreal forest, *Tellus B*, 50, 449-462, 1998.

Kulmala, M. and Kerminen, V.-M.: On the formation and growth of atmospheric nanoparticles, *Atmos. Res.*, 90, 132–150, 2008.

Kumar, P., Morawska, L., Birmili, W., Paasonen, P., Hu, M., Kulmala, M., Harrison, R. M., Norford, L. and Britter, R.: Ultrafine particles in cities, *Environ.Int.*, 66, 1-10, 2014.

Kumar, P., Pirjola, L., Ketzel, M. and Harrison, R M.: Nanoparticle emissions from 11 non-vehicle exhaust sources—A review, *Atmos.Environ.*, 67, 252-277, 2013.

Lanzinger, S., Schneider, A., Breitner, S., Stafoggia, M., Erzen, I., Dostal, M., Pastorkova, A., Bastian, S., Cyrus, J., Zscheppang, A. and Kolodnitska, T.: Associations between ultrafine and fine particles and mortality in five central European cities—Results from the UFIRES study, *Environ. Int.*, 88, 44-52, 2016.

Lee, D. S., Fahey, D. W., Forster, P. M., Newton, P. J., Wit, R. C. N., Lim, L. L., Owen, B., Sausen and R.: Aviation and global climate change in the 21st century, *Atmos. Environ.*, 43, 3520-3537, 2009.

Liu, X., Wang, W., Liu, H., Geng, C., Zhang, W., Wang, H. and Liu, Z.: Number size distribution of particles emitted from two kinds of typical boilers in a coal-fired power plant in China, *Eng. Fuels*, 24, 1677-1681, 2010.

Liu, Z. R., Hu, B., Liu, Q., Sun, Y. and Wang, Y. S.: Source apportionment of urban fine particle number concentration during summertime in Beijing, *Atmos. Environ.*, 96, 359-369, 2014.

Lobo, P., Hagen, D. E. and Whitefield, P. D.: Measurement and analysis of aircraft engine PM emissions downwind of an active runway at the Oakland International Airport, *Atmos. Environ.*, 61, 114-123, 2012.

Lobo, P., Hagen, D. E., Whitefield, P. D. and Raper, D.: PM emissions measurements of in-service commercial aircraft engines during the Delta-Atlanta Hartsfield Study, *Atmos. Environ.*, 104, 237-245, 2015.

Lupu, A. and Maenhaut, W.: Application and comparison of two statistical trajectory techniques for identification of source regions of atmospheric aerosol species, *Atmos. Environ.*, 36, 5607-5618, 2002.

Masiol, M. and Harrison, R. M.: Aircraft engine exhaust emissions and other airport-related contributions to ambient air pollution: A review, *Atmos. Environ.*, 95, 409-455, 2014.

Masiol, M. and Harrison, R.M.: Quantification of air quality impacts of London Heathrow Airport (UK) from 2005 to 2012, *Atmos. Environ.*, 116, 308-319, 2015.



1181 Masiol, M., Vu, V. T., Beddows, D. C. S. and Harrison, R.M.: Source apportionment of wide range  
 1182 particle size spectra and black carbon collected at the airport of Venice (Italy), *Atmos. Environ.*,  
 1183 139, 56-74, 2016.

1184

1185 Masiol M., Hopke P. K., Felton H. D., Frank B. P., Rattigan O. V., Wurth M. J. and LaDuke G. H.:  
 1186 Source apportionment of PM<sub>2.5</sub> chemically speciated mass and particle number concentrations in  
 1187 New York City, *Atmos. Environ.*, 148, 215-229, 2017.

1188

1189 Mazaheri, M., Johnson, G. R. and Morawska, L.: Particle and gaseous emissions from commercial  
 1190 aircraft at each stage of the landing and takeoff cycle, *Environ. Sci. Technol.*, 43, 441-446, 2009.

1191

1192 Mazaheri, M., Bostrom, T. E., Johnson, G. R. and Morawska, L.: Composition and morphology of  
 1193 particle emissions from in-use aircraft during takeoff and landing, *Environ. Sci. Technol.*, 47, 5235-  
 1194 5242, 2013.

1195

1196 Meyer, N. K. and Ristovski, Z.: Ternary nucleation as a mechanism for the production of diesel  
 1197 nanoparticles: experimental analysis of the volatile and hygroscopic properties of diesel exhaust  
 1198 using the volatilization and humidification tandem differential mobility analyser, *Environ. Sci.*  
 1199 *Technol.*, 41, 7309-7314, 2007.

1200

1201 Ntziachristos, L., Ning, Z. Geller, M. D. and Sioutas, C.: Particle concentration and characteristics  
 1202 near a major freeway with heavy-duty diesel traffic, *Environ. Sci. Technol.*, 41, 2223-2230, 2007.

1203

1204 O'Dowd, C. D., Geever, M., Hill, M. K., Smith, M. H. and Jennings, S. G.: New particle formation:  
 1205 Nucleation rates and spatial scales in the clean marine coastal environment, *Geophys. Res. Lett.*, 25,  
 1206 1661-1664, 1998.

1207

1208 O'Dowd, C., McFiggans, G., Creasey, D. J., Pirjola, L., Hoell, C., Smith, M. H., Allan, B. J., Plane,  
 1209 J. M. C., Heard, D. E., Lee, J. D., Pilling, M. J. and Kulmala, M.: On the photochemical production  
 1210 of new particles in the coastal boundary layer. *Geophys. Res. Lett.*, 26, 1707-1710, 1999.

1211

1212 Ogulei, D., Hopke, P. K., Chalupa, D. C. and Utell, M. J.: Modeling source contributions to  
 1213 submicron particle number concentrations measured in Rochester, New York, *Aerosol Sci.*  
 1214 *Technol.*, 41, 179-201, 2007.

1215 Ostro, B., Hu, J., Goldberg, D., Reynolds, P., Hertz, A., Bernstein, L. and Kleeman, M. J.:  
 1216 Associations of mortality with long-term exposures to fine and ultrafine particles, species and  
 1217 sources: Results from the California Teachers Study Cohort, *Environ. Health Perspect.*, 123, 549-  
 1218 556, 2015.

1219

1220 Paatero, P.: Least squares formulation of robust non-negative factor analysis, *Chemom. Intell. Lab.*,  
 1221 37, 23-35, 1997.

1222

1223 Paatero, P. and Tapper, U.: Positive matrix factorization: a non-negative factor model with optimal  
 1224 utilization of error estimates of data values, *Environmetrics*, 5, 111-126, 1994.

1225

1226 Paatero, P., Hopke, P. K., Song, X. H. and Ramadan, Z.: Understanding and controlling rotations in  
 1227 factor analytic models, *Chemom. Intell. Lab. Syst.*, 60, 253-264, 2002.

1228

1229 Paatero, P., Eberly, S., Brown, S. G. and Norris, G. A.: Methods for estimating uncertainty in  
 1230 factor analytic solutions., *Atmos. Meas. Tech.*, 7, 781-797, 2014.

1231

1232 Pant, P. and Harrison, R. M.: Estimation of the contribution of road traffic emissions to particulate  
1233 matter concentrations from field measurements: a review, *Atmos. Environ.*, 77, 78-97, 2013.  
1234

1235 Petzold, A., Ogren, J.A., Fiebig, M., Laj, P., Li, S.M., Baltensperger, U., Holzer-Popp, T., Kinne,  
1236 S., Pappalardo, G., Sugimoto, N. and Wehrli, C., Wiedensohler, A., Zhang, X.-Y.:  
1237 Recommendations for reporting "black carbon" measurements, *Atmos. Chem. Phys.*, 13, 8365-  
1238 8379, 2013.  
1239

1240 R Core Team: R: A language and environment for statistical computing. R Foundation for  
1241 Statistical Computing, Vienna, Austria, 2015. URL <http://www.R-project.org/>.  
1242

1243 Reff, A., Eberly, S. I. and Bhawe, P. V.: Receptor modeling of ambient particulate matter data using  
1244 positive matrix factorization: review of existing methods, *JAWMA*, 57, 146-154, 2007.  
1245

1246 Ren, J., Liu, J., Li, F., Cao, X., Ren, S., Xu, B. and Zhu, Y.: A study of ambient fine particles at  
1247 Tianjin International Airport, China, *Sci. Total Environ.*, 556, 126-135, 2016.  
1248

1249 Riccobono, F., Schobesberger, S., Scott, C. E., Dommen, J., Ortega, I. K., Rondo, L., Almeida, J.,  
1250 Amorim, A., Bianchi, F., Breitenlechner, M. And David, A.: Oxidation products of biogenic  
1251 emissions contribute to nucleation of atmospheric particles, *Science*, 344, 717-721, 2014.  
1252

1253 Rolph, G. D.: Real-time Environmental Applications and Display sYstem (READY) Website,  
1254 <http://www.ready.noaa.gov>, NOAA Air Resources Laboratory, College Park, MD, 2016.  
1255

1256 Salimi, F., Ristovski, Z., Mazaheri, M., Laiman, R., Crilley, L. R., He, C., Clifford, S. and  
1257 Morawska, L.: Assessment and application of clustering techniques to atmospheric particle number  
1258 size distribution for the purpose of source apportionment, *Atmos. Chem. Phys.*, 14, 11883-11892,  
1259 2014.  
1260

1261 Salma, I., Fűri, P., Németh, Z., Balásházy, I., Hofmann, W. and Farkas, Á.: Lung burden and  
1262 deposition distribution of inhaled atmospheric urban ultrafine particles as the first step in their  
1263 health risk assessment, *Atmos. Environ.*, 104, 39-49, 2015.  
1264

1265 Sandradewi, J., Prévôt, A. S., Szidat, S., Perron, N., Alfarra, M. R., Lanz, V. A., Weingartner, E.  
1266 and Baltensperger, U.: Using aerosol light absorption measurements for the quantitative  
1267 determination of wood burning and traffic emission contributions to particulate matter, *Environ.*  
1268 *Sci. Technol.*, 42, 3316-3323, 2008.  
1269

1270 Schneider, J., Hock, N., Weimer, S., Borrmann, S., Kirchner, U., Vogt, R. and Scheer, V.:  
1271 Nucleation particles in diesel exhaust: Composition inferred from in situ mass spectrometric  
1272 analysis, *Environ. Sci. Technol.*, 39, 6153-6161, 2005.  
1273

1274 Seinfeld, J. H. and Pandis, S. N.: *Atmospheric Chemistry and Physics - From Air Pollution to*  
1275 *Climate Change*, second ed., John Wiley & Sons, New York, 2006.  
1276

1277 Shi, J. P. and Harrison, R. M.: Investigation of ultrafine particle formation during diesel exhaust  
1278 dilution, *Environ. Sci. Technol.*, 33, 3730-3736, 1999.  
1279

1280 Shi, L., Zanobetti, A., Kloog, I., Coull, B. A., Koutrakis, P., Melly, S. J. and Schwartz, J. D.: Low-  
1281 concentration PM<sub>2.5</sub> and mortality: Estimating acute and chronic effects in a population-based  
1282 study, *Environ. Health Perspect.*, 124, 46-52, 2015.  
1283

1284 Shirmohammadi, F., Sowlat, M. H., Hasheminassab, S., Saffari, A., Ban-Weiss, G. and Sioutas, C.:  
 1285 Emission rates of particle number, mass and black carbon by the Los Angeles International Airport  
 1286 (LAX) and its impact on air quality in Los Angeles, *Atmos. Environ.*, 151, 82-93, 2017.  
 1287  
 1288 Sowlat M.H., Hasheminassab S. and Sioutas C.: Source apportionment of ambient particle number  
 1289 concentrations in central Los Angeles using positive matrix factorization (PMF), *Atmos. Chem.*  
 1290 *Phys.*, 16, 4849-4866, 2016.  
 1291  
 1292 Squizzato, S. and Masiol, M.: Application of meteorology-based methods to determine local and  
 1293 external contributions to particulate matter pollution: A case study in Venice (Italy), *Atmos.*  
 1294 *Environ.*, 119, 69-81, 2015.  
 1295  
 1296 Stein, A. F., Draxler, R. R., Rolph, G. D., Stunder, B. J. B., Cohen, M. D. and Ngan, F.: NOAA's  
 1297 HYSPLIT atmospheric transport and dispersion modeling system, *Bull. Amer. Meteor. Soc.*, 96,  
 1298 2059-2077, 2015.  
 1299  
 1300 Stevens, R. G., Pierce, J. R., Brock, C. A., Reed, M. K., Crawford, J. H., Holloway, J. S., Ryerson,  
 1301 T. B., Huey, L. G. and Nowak, J. B.: Nucleation and growth of sulfate aerosol in coal-fired power  
 1302 plant plumes: sensitivity to background aerosol and meteorology, *Atmos. Chem. Phys.*, 12, 189-  
 1303 206, 2012.  
 1304  
 1305 Stohl A.: Trajectory statistics—a new method to establish source–receptor relationships of air  
 1306 pollutants and its application to the transport of particulate sulfate in Europe, *Atmos. Environ.*, 30,  
 1307 579-587, 1996.  
 1308  
 1309 Stohl, A.: Computation, accuracy and applications of trajectories- review and bibliography, *Atmos.*  
 1310 *Environ.*, 32, 947-966, 1998.  
 1311  
 1312 Stafoggia, M., Cattani, G., Forastiere, F., di Bucchianico, A. D. M., Gaeta, A. And Ancona, C.:  
 1313 Particle number concentrations near the Rome-Ciampino city airport, *Atmos. Environ.*, 147, 264-  
 1314 273, 2016.  
 1315  
 1316 Strak, M. M., Janssen, N. A., Godri, K. J., Gosens, I., Mudway, I. S., Cassee, F. R., Lebret, E.,  
 1317 Kelly, F. J., Harrison, R. M., Brunekreef, B. and Steenhof, M.: Respiratory health effects of  
 1318 airborne particulate matter: the role of particle size, composition, and oxidative potential-the  
 1319 RAPTES project, *Environ. Health Perspect.*, 120, 1183-1189, 2012.  
 1320  
 1321 Thimmaiah, D., Hovorka, J. and Hopke, P. K.: Source apportionment of winter submicron Prague  
 1322 aerosols from combined particle number size distribution and gaseous composition data. *Aerosol*  
 1323 *Air Qual.Res.*, 9, 209-236, 2009.  
 1324  
 1325 Turner, J.R., Hansen, A.D.A., and Allen G.A.: Methodologies to compensate for optical saturation  
 1326 and scattering in aethalometer black carbon measurements, in: *Proceedings from the Symposium on*  
 1327 *Air Quality Measurement Methods and Technology*, San Francisco, CA, USA, 30 April-3 May  
 1328 2007, Air and Waste Management Association, 2007.  
 1329  
 1330 UK Department for Transport, Heathrow Airport expansion:  
 1331 <https://www.gov.uk/government/collections/heathrow-airport-expansion>, last access: 20 June  
 1332 2017.  
 1333  
 1334 USEPA: EPA Positive Matrix Factorization (PMF) 5.0 - Fundamentals and user guide.  
 1335 EPA/600/R-14/108, 2014

1336  
1337 Virkkula, A., Mäkelä, T., Hillamo, R., Yli-Tuomi, T., Hirsikko, A., Hämeri, K. and Koponen, I.K.:  
1338 A simple procedure for correcting loading effects of aethalometer data, *J. Air Waste Manage.*  
1339 *Assoc.*, 57, 1214-1222, 2007.  
1340  
1341 Vogt, R., Scheer, V., Casati, R. and Benter, T.: Onroad measurement of particle emission in the  
1342 exhaust plume of a diesel passenger car, *Environ. Sci. Technol.*, 37, 4070-4076, 2003.  
1343  
1344 von Bismarck-Osten, C., Birmili, W., Ketzel, M., Massling, A., Petäjä, T. and Weber, S.:  
1345 Characterization of parameters influencing the spatio-temporal variability of urban particle number  
1346 size distributions in four European cities, *Atmos. Environ.*, 77, 415-429, 2013.  
1347  
1348 Vu, T. V., Delgado-Saborit, J. M. and Harrison, R. M.: A review of hygroscopic growth factors of  
1349 submicron aerosols from different sources and its implication for calculation of lung deposition  
1350 efficiency of ambient aerosols, *Air Quality, Atmos. Health*, 8, 429-440, 2015a.  
1351  
1352 Vu, T. V., Delgado-Saborit, J. M. and Harrison, R. M.: Review: Particle number size distributions  
1353 from seven major sources and implications for source apportionment studies, *Atmos. Environ.*, 122,  
1354 114-132, 2015b.  
1355  
1356 Vu, T. V., Beddows, D. C. S., Delgado-Saborit, J. M. and Harrison, R. M.: Source Apportionment  
1357 of the Lung Dose of Ambient Submicrometre Particulate Matter, *Aerosol Air Quality Res.*, doi:  
1358 10.4209/aaqr.2015.09.0553, 2016  
1359  
1360 Yin, J., Harrison, R. M., Chen, Q., Rutter, A. and Schauer, J. J.: Source apportionment of fine  
1361 particles at urban background and rural sites in the UK atmosphere, *Atmos. Environ.*, 44, 841-851,  
1362 2010.  
1363  
1364 Yue, W., Stolzel, M., Cyrys, J., Pitz, M., Heinrich, J., Kreyling, W. G., Wichmann, H.-E., Peters, A.,  
1365 Wang, S. and Hopke, P.K.: Source apportionment of ambient fine particle size distribution using  
1366 positive matrix factorization in Erfurt, Germany, *Sci. Total Environ.*, 398, 133-144, 2008.  
1367  
1368 Wang, Y., Hopke, P. K., Rattigan, O. V., Xia, X., Chalupa, D. C., Utell, M. J.: Characterization of  
1369 residential wood combustion particles using the two-wavelength aethalometer, *Environ.Sci.*  
1370 *Technol.*, 45, 7387-7393, 2011.  
1371  
1372 Webb, S., Whitefield, P. D., Miake-Lye, R. C., Timko, M. T. and Thrasher, T. G.: Research needs  
1373 associated with particulate emissions at airports, ACRP Report 6, Transportation Research Board,  
1374 Washington, D.C., 2008.  
1375  
1376 Wehner, B., Uhrner, U., Von Löwis, S., Zallinger, M. and Wiedensohler, A.: Aerosol number size  
1377 distributions within the exhaust plume of a diesel and a gasoline passenger car under on-road  
1378 conditions and determination of emission factors, *Atmos. Environ.*, 43, 1235-1245, 2009.  
1379  
1380 Wegner, T., Hussein, T., Hämeri, K., Vesala, T., Kulmala, M. and Weber, S.: Properties of aerosol  
1381 signature size distributions in the urban environment as derived by cluster analysis, *Atmos.*  
1382 *Environ.*, 61, 350-360, 2012.  
1383  
1384 Westerdahl, D., Fruin, S.A., Fine, P.L. and Sioutas, C.: The Los Angeles International Airport as a  
1385 source of ultrafine particles and other pollutants to nearby communities, *Atmos. Environ.*, 42(13),  
1386 3143-3155, 2008.  
1387

1388 Wormhoudt, J., Herndon, S. C., Yelvington, P. E., Lye-Miake, R. C. and Wey, C.: Nitrogen oxide  
 1389 (NO/NO<sub>2</sub>/HONO) emissions measurements in aircraft exhausts, *J. Propul. Power*, 23, 906-911,  
 1390 2007.  
 1391  
 1392 Zhang, K. M., Wexler, A. S., Zhu, Y. F., Hinds, W. C. and Sioutas, C.: Evolution of particle  
 1393 number distribution near roadways. Part II: the 'Road-to-Ambient' process, *Atmos. Environ.*, 38,  
 1394 6655-6665, 2004.  
 1395  
 1396 Zhang, K. M., Wexler, A. S., Niemeier, D. A., Zhu, Y. F., Hinds, W. C. and Sioutas, C.: Evolution  
 1397 of particle number distribution near roadways. Part III: Traffic analysis and on-road size resolved  
 1398 particulate emission factors, *Atmos. Environ.*, 39, 4155-4166, 2005.  
 1399  
 1400 Zhang, R., Khalizov, A., Wang, L., Hu, M. and Xu, W.: Nucleation and growth of nanoparticles in  
 1401 the atmosphere, *Chem. Rev.*, 112, 1957-2011, 2011.  
 1402  
 1403 Zhou, L., Hopke, P. K., Stanier, C. O., Pandis, S. N., Ondov, J. M. and Pancras, J. P.: Investigation  
 1404 of the relationship between chemical composition and size distribution of airborne particles by  
 1405 partial least squares and positive matrix factorization, *J. Geophys. Res.-Atmos.*, 110, D07S18, 2005,  
 1406 doi:10.1029/2004JD005050.  
 1407  
 1408 Zíková, N., Wang, Y., Yang, F., Li, X., Tian, M. and Hopke, P. K.: On the source contribution to  
 1409 Beijing PM 2.5 concentrations, *Atmos. Environ.*, 134, 84-95, 2016.  
 1410  
 1411

1412 **TABLE LEGENDS:**

1413

1414 **Table 1.** Summary of PMF results for both seasons.

1415

1416 **Table 2.** Results of Pearson's correlation analysis among extracted factor contributions and  
 1417 other measured variables recorded at different time resolutions. Only correlations  
 1418 significant at  $p < 0.05$  are reported, strong correlations ( $\rho > |0.6|$ ) are highlighted in bold.

1419

1420

1421 **FIGURE LEGENDS:**

1422

1423 **Figure 1.** Statistics of size distribution spectra for particle number (red) and volume (blue)  
 1424 concentrations categorised by sampling periods and time of the day (daytime= 7am-  
 1425 7pm and nighttime=7pm- 7am local time). For the particle number spectra, solid lines  
 1426 represent the median concentrations, while shaded areas report the 1st-3rd quartile  
 1427 intervals (interquartile range, IQR). For the particle volume spectra, only medians are  
 1428 reported (dotted lines).

1429

1430 **Figure 2.** Diurnal patterns of PNC, LHR traffic, solar irradiance and eBC. Plots report the  
 1431 average levels as a filled line and the associated 95th confidence interval calculated by  
 1432 bootstrapping the data (n= 200). Outliers (data >99.5th percentile) were removed for  
 1433 computing the diurnal patterns. Hours are given in UTC. LHR traffic movements  
 1434 (bottom right plot) are reported as arrivals (dotted lines) and departures (solid lines).  
 1435 The offset between the seasons is largely due to daylight saving time (BST = UTC +  
 1436 1) in the summer data. The diurnal patterns of all the measured variables in reported in  
 1437 Figure SI4.

1438

1439 **Figure 3.** Results of cluster analysis for the warm season data. Average cluster PNSD spectra  
 1440 (left) are reported as solid red lines along with: (i) their 10th, 25th, 75th and 90th  
 1441 percentile spectrum as shaded areas; (ii) the volume size distributions (dotted blue  
 1442 line); (iii) the hourly counts and (iv) the wind roses associated with each cluster.

1443

1444 **Figure 4.** Results of cluster analysis for the cold season data. Average cluster PNSD spectra  
 1445 (left) are reported as solid red lines along with: (i) their 10th, 25th, 75th and 90th  
 1446 percentile spectrum as shaded areas; (ii) the volume size distributions (dotted blue  
 1447 line); (iii) the hourly counts and (iv) the wind roses associated with each cluster.

1448

1449 **Figure 5.** Results of PMF analysis for the warm season data. Factor profiles are reported on the  
 1450 left as: (i) number concentration in solid red lines; (ii) their DISP ranges in shaded red  
 1451 areas; (iii) volume concentrations in dotted blue lines; (iv) explained variation in  
 1452 dashed grey lines. The plots on the centre report the normalised daily patterns  
 1453 calculated on the hourly-averaged factor contributions along with their 95th  
 1454 confidence intervals (n=200 bootstrap). The plots on the right show the polar plot  
 1455 analysis (normalised average factor contributions). SA=secondary aerosol.

1456

1457 **Figure 6.** Results of PMF analysis for the cold season data. Factor profiles are reported on the  
 1458 left as: (i) number concentration in solid red lines; (ii) their DISP ranges in shaded red  
 1459 areas; (iii) volume concentrations in dotted blue lines; (iv) explained variation in  
 1460 dashed grey lines. The plots on the centre report the normalised daily patterns  
 1461 calculated on the hourly-averaged factor contributions along with their 95th

confidence intervals (n=200 bootstrap). The plots on the right show the polar plot analysis (normalised average factor contributions). SA=secondary aerosol.

**Figure 7.** CWT maps of the secondary aerosol-related factors for both the seasons. Map scales refer to the average factor contributions to the total variable (PNC).

**Figure 8.** Comparison of k-means and PMF for the warm (upper plots) and cold (bottom plots) seasons. Boxplot statistics: lines= medians, crosses= arithmetic means, boxes= 25th-75th percentile ranges, whiskers=  $\pm 1.5$ \*inter-quartile ranges.

**Figure 9.** Analysis of the regional nucleation episode occurring on September 7th. The selected period is from 7 September midnight to 8 September 4 pm. The plots represent (from upper to the bottom): (a) contour plots of SMPS data; (b) Concentrations of some measured species (Nucl= particles in the nucleation range 14-30 nm; Ait= particles in the Aitken Nuclei range 30-100 nm; Acc= particles in the accumulation range >100 nm; mass of PM<sub>2.5</sub>); (c) Source contributions from PMF for the Factors 1, 2, 3 and 4; (d) hourly counts of number of clusters. The arrows in the (b) and (c) plots show the wind direction (arrow direction) and speed (proportional to arrow length).

1482 **Table 1.** Summary of PMF results for both seasons.

1483

Factor number and interpretation	Particle Number Concentration		Particle Volume Concentration	
	No. modes <sup>a</sup> (peak ranges <sup>b</sup> )	Percent contribution (DISP range)	No. modes <sup>a</sup> (peak ranges <sup>b</sup> )	Percent contribution
<b>Warm season</b> (Aug-Sep 2014)				
<b>Factor 1: Airport</b>	1 (<20 nm)	31.6 (30.8–36.2)	2 (60–160 nm; <25 nm)	1.2
<b>Factor 2: Fresh road traffic</b>	1 (20–35 nm)	27.9 (24.7–30.2)	2 (22–45 nm; 140–220 nm)	1.7
<b>Factor 3: Aged road traffic</b>	1 (30–60 nm)	18.9 (16.6–21.1)	2 (40–100 nm; 250–450 nm)	5.6
<b>Factor 4: Urban accumulation</b>	1 (50–150 nm)	14.4 (13.8–18)	1 (80–250 nm)	33.2
<b>Factor 5: Mixed SA<sup>c</sup></b>	1 (110–250 nm)	5.2 (3.6–6.9)	1 (160–350 nm)	37.4
<b>Factor 6: Inorganic SA</b>	2 (55–120 nm; 230–400 nm)	2.1 (1.1–3.5)	2 (260–500 nm; 75–140 nm)	20.8
<b>Cold season</b> (Dec 2014-Jan 2015)				
<b>Factor 1: Airport</b>	1 (<20 nm)	33.1 (31.7–34.8)	2 (160–350 nm; 15–25 nm)	1.7
<b>Factor 2: Fresh road traffic</b>	1 (18–35 nm)	35.2 (33.4–36.9)	2 (22–45 nm; 150–300 nm)	3.1
<b>Factor 3: Aged road traffic</b>	1 (28–60 nm)	18.9 (17.9–19.7)	2 (40–150 nm; 330–450 nm)	8.7
<b>Factor 4: Urban accumulation</b>	1 (55–170 nm)	7.6 (7.3–8.3)	1 (100–250 nm)	32.5
<b>Factor 5: Mixed SA</b>	2 (130–280 nm, <17 nm)	2.3 (2.1–3.3)	1 (170–400 nm)	30.8
<b>Factor 6: Inorganic SA</b>	3 (17–28 nm; 55–100 nm, 250–400 nm)	2.9 (2.4–3.9)	2 (280–550 nm; 90–140 nm)	23.3

(a) Only modes above the DISP ranges are shown; (b) Range endpoints are taken at approx. half the mode height;

(c) SA = secondary aerosol

1484



**Table 2.** Results of Pearson's correlation analysis among extracted factor contributions and other measured variables recorded at different time resolutions. Only correlations significant at  $p < 0.05$  are reported, strong correlations ( $\rho > |0.6|$ ) are highlighted in bold.

Variables	Warm period					
	Factor 1	Factor 2	Factor 3	Factor 4	Factor 5	Factor 6
	Airport	Fresh road traffic	Aged road traffic	Urban accumulation	Mixed SA	Inorganic SA
<i>Weather parameters (1 h-resolution time)</i>						
Solar irr.	0.12	-0.15	-0.24	-0.26	-0.24	-0.28
Air temp.	0.25	-0.21	-0.37	-0.1	0.1	
RH		0.1	0.32	0.22	0.26	0.33
Wind speed	0.38		-0.47	<b>-0.64</b>	-0.45	-0.49
<i>5 min-resolution time</i>						
Factor 1	–					
Factor 2	0.46	–				
Factor 3	0.03	0.28	–			
Factor 4	-0.17	-0.04	0.47	–		
Factor 5	-0.15	-0.06	0.21	0.56	–	
Factor 6	-0.17	-0.14	0.15	0.56	<b>0.75</b>	–
eBC	-0.1	-0.03	0.33	<b>0.62</b>	0.52	0.53
Delta-C			0.13	-0.07		-0.06
<i>1 h-resolution time</i>						
NO			0.43	<b>0.6</b>	0.32	0.33
NO <sub>2</sub>		0.18	<b>0.61</b>	<b>0.76</b>	0.52	0.52
NO <sub>x</sub>		0.11	0.58	<b>0.77</b>	0.48	0.48
O <sub>3</sub>	0.14	-0.19	-0.57	-0.54	-0.37	-0.43
PM <sub>2.5</sub>	-0.23	-0.24	0.13	<b>0.61</b>	<b>0.63</b>	<b>0.77</b>
NVPM <sub>2.5</sub>	-0.22	-0.22	0.17	<b>0.62</b>	<b>0.61</b>	<b>0.75</b>
VPM <sub>2.5</sub>	-0.17	-0.24		0.42	0.54	<b>0.65</b>
<i>1 day-resolution time PM<sub>2.5</sub>-bound species</i>						
OC				<b>0.84</b>	<b>0.74</b>	<b>0.83</b>
EC	-0.47	-0.54		<b>0.75</b>	0.51	<b>0.67</b>
TC	-0.45	-0.44		<b>0.85</b>	<b>0.69</b>	<b>0.82</b>
Chloride						
Nitrate		-0.45			<b>0.83</b>	<b>0.85</b>
Sulphate		-0.57		<b>0.75</b>	0.5	<b>0.67</b>
Oxalate		-0.47		0.59	<b>0.89</b>	<b>0.93</b>
Sodium						
Ammonium	-0.44	-0.52		0.57	0.54	<b>0.71</b>
Potassium		-0.47		0.46	0.5	<b>0.66</b>
Magnesium	0.5			-0.53		
Calcium						

1490 **Table 2.** Continued.

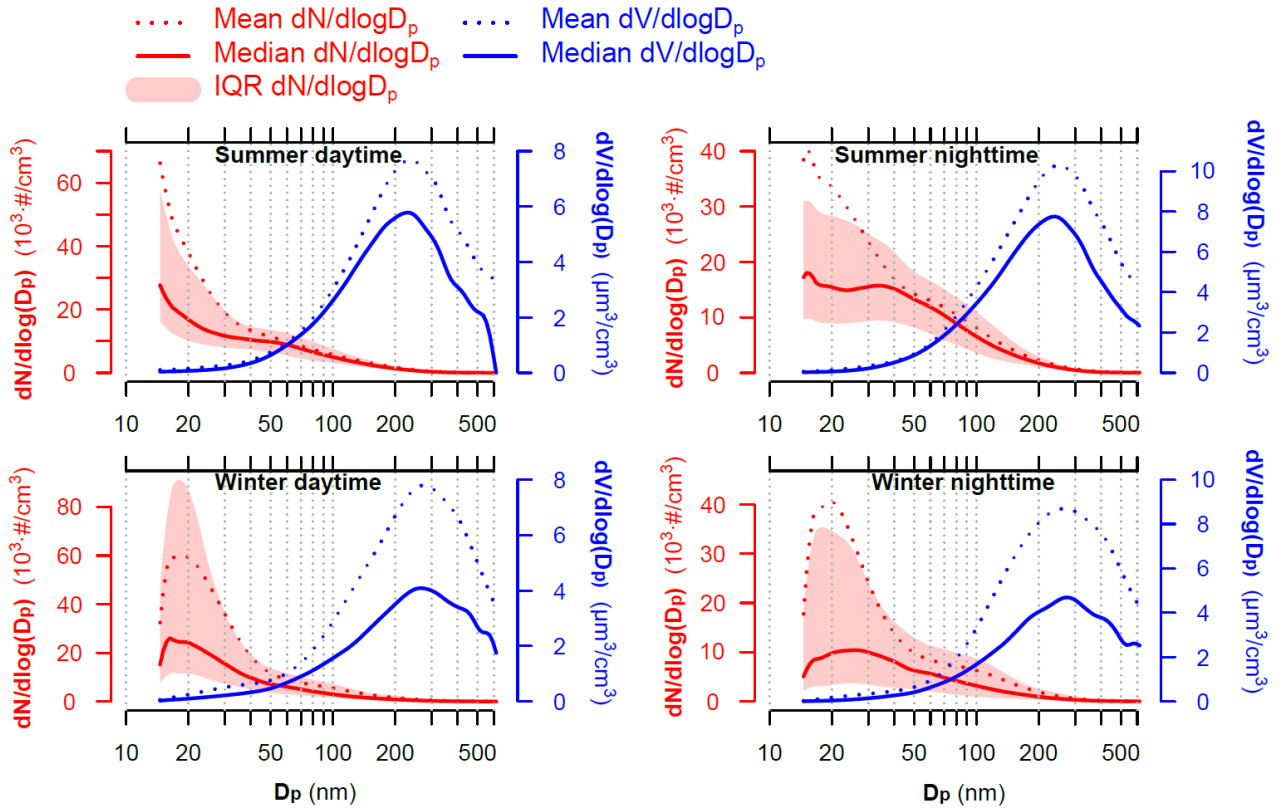
1491

Variables	Factor 1	Factor 2	Cold period		Factor 5	Factor 6
	Airport	Fresh road traffic	Aged road traffic	Urban accumulation	Mixed SA	Inorganic SA
<i>Weather parameters (1 h-resolution time)</i>						
<b>Solar irr.</b>				-0.11		
<b>Air temp.</b>	0.38		-0.43	<b>-0.67</b>	-0.5	-0.59
<b>RH</b>			0.23	0.38	0.46	0.46
<b>Wind speed</b>	0.3		-0.49	<b>-0.67</b>	-0.54	<b>-0.61</b>
<i>5 min-resolution time</i>						
<b>Factor 1</b>	–					
<b>Factor 2</b>	0.55	–				
<b>Factor 3</b>	0.24	0.54	–			
<b>Factor 4</b>	-0.11	0.08	0.53	–		
<b>Factor 5</b>	-0.05	0.15	0.38	<b>0.65</b>	–	
<b>Factor 6</b>	-0.09	0.08	0.39	<b>0.7</b>	<b>0.81</b>	–
<b>eBC</b>		0.16	0.52	<b>0.77</b>	<b>0.60</b>	<b>0.63</b>
<b>Delta-C</b>			0.35	<b>0.62</b>	0.55	0.52
<i>1 h-resolution time</i>						
<b>NO</b>	-0.14		0.51	<b>0.81</b>	<b>0.62</b>	<b>0.63</b>
<b>NO<sub>2</sub></b>	0.13	0.42	<b>0.81</b>	<b>0.82</b>	<b>0.61</b>	<b>0.66</b>
<b>NO<sub>x</sub></b>		0.17	<b>0.63</b>	<b>0.85</b>	<b>0.64</b>	<b>0.68</b>
<b>O<sub>3</sub></b>		-0.29	<b>-0.71</b>	<b>-0.78</b>	<b>-0.65</b>	<b>-0.7</b>
<b>PM<sub>2.5</sub></b>	-0.1	0.16	0.53	<b>0.82</b>	<b>0.88</b>	<b>0.88</b>
<b>NVPM<sub>2.5</sub></b>	-0.11	0.16	0.53	<b>0.82</b>	<b>0.85</b>	<b>0.85</b>
<b>VPM<sub>2.5</sub></b>			0.19	0.39	0.49	0.48
<i>1 day-resolution time PM<sub>2.5</sub>-bound species</i>						
<b>OC</b>			<b>0.79</b>	<b>0.79</b>	<b>0.76</b>	<b>0.8</b>
<b>EC</b>			<b>0.83</b>	<b>0.8</b>	<b>0.64</b>	<b>0.66</b>
<b>TC</b>			<b>0.81</b>	<b>0.8</b>	<b>0.73</b>	<b>0.77</b>
<b>Chloride</b>				0.58	<b>0.82</b>	<b>0.85</b>
<b>Nitrate</b>		<b>0.63</b>	<b>0.73</b>	<b>0.88</b>	<b>0.93</b>	<b>0.9</b>
<b>Sulphate</b>					<b>0.92</b>	<b>0.88</b>
<b>Oxalate</b>					<b>0.87</b>	<b>0.81</b>
<b>Sodium</b>		-0.58	<b>-0.74</b>	<b>-0.64</b>		
<b>Ammonium</b>			<b>0.63</b>	<b>0.78</b>	<b>0.99</b>	<b>0.97</b>
<b>Potassium</b>				<b>0.71</b>	<b>0.98</b>	<b>0.97</b>
<b>Magnesium</b>						
<b>Calcium</b>						

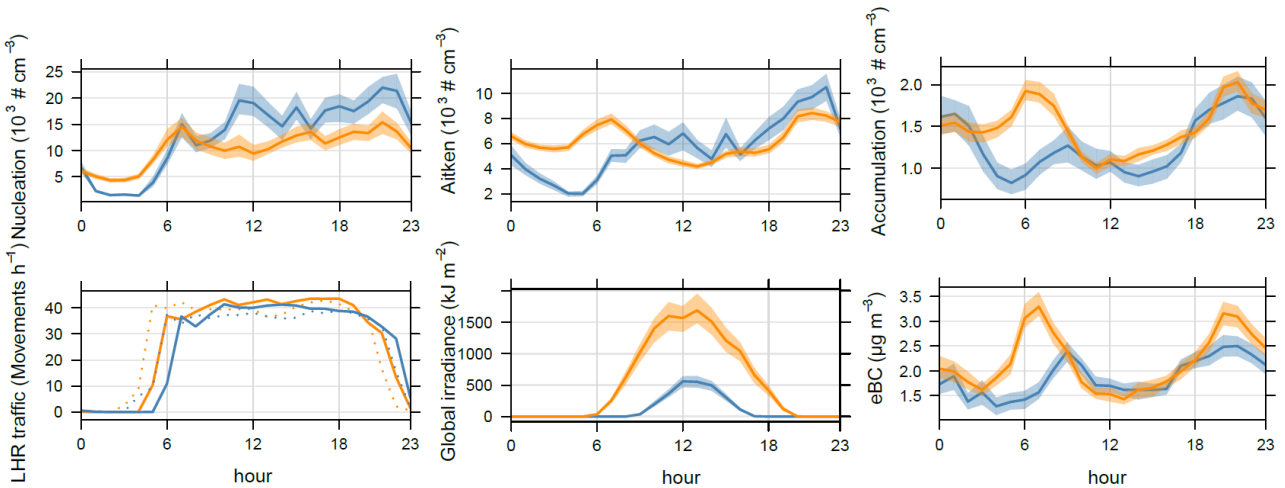
1492

1493

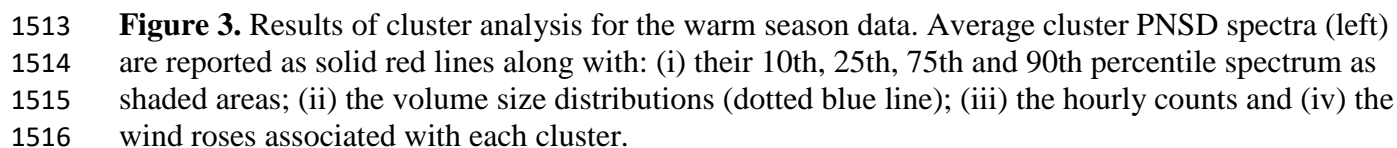
1494



**Figure 1.** Statistics of size distribution spectra for particle number (red) and volume (blue) concentrations categorised by sampling periods and time of the day (daytime= 7am-7pm and nighttime=7pm- 7am local time). For the particle number spectra, solid lines represent the median concentrations, while shaded areas report the 1st-3rd quartile intervals (interquartile range, IQR). For the particle volume spectra, only medians are reported (dotted lines).



**Figure 2.** Diurnal patterns of PNC, LHR traffic, solar irradiance and eBC. Plots report the average levels as a filled line and the associated 95th confidence interval calculated by bootstrapping the data ( $n = 200$ ). Outliers (data  $> 99.5$ th percentile) were removed for computing the diurnal patterns. Hours are given in UTC. LHR traffic movements (bottom right plot) are reported as arrivals (dotted lines) and departures (solid lines). The offset between the seasons is largely due to daylight saving time (BST = UTC + 1) in the summer data. The diurnal patterns of all the measured variables in reported in Figure SI4.



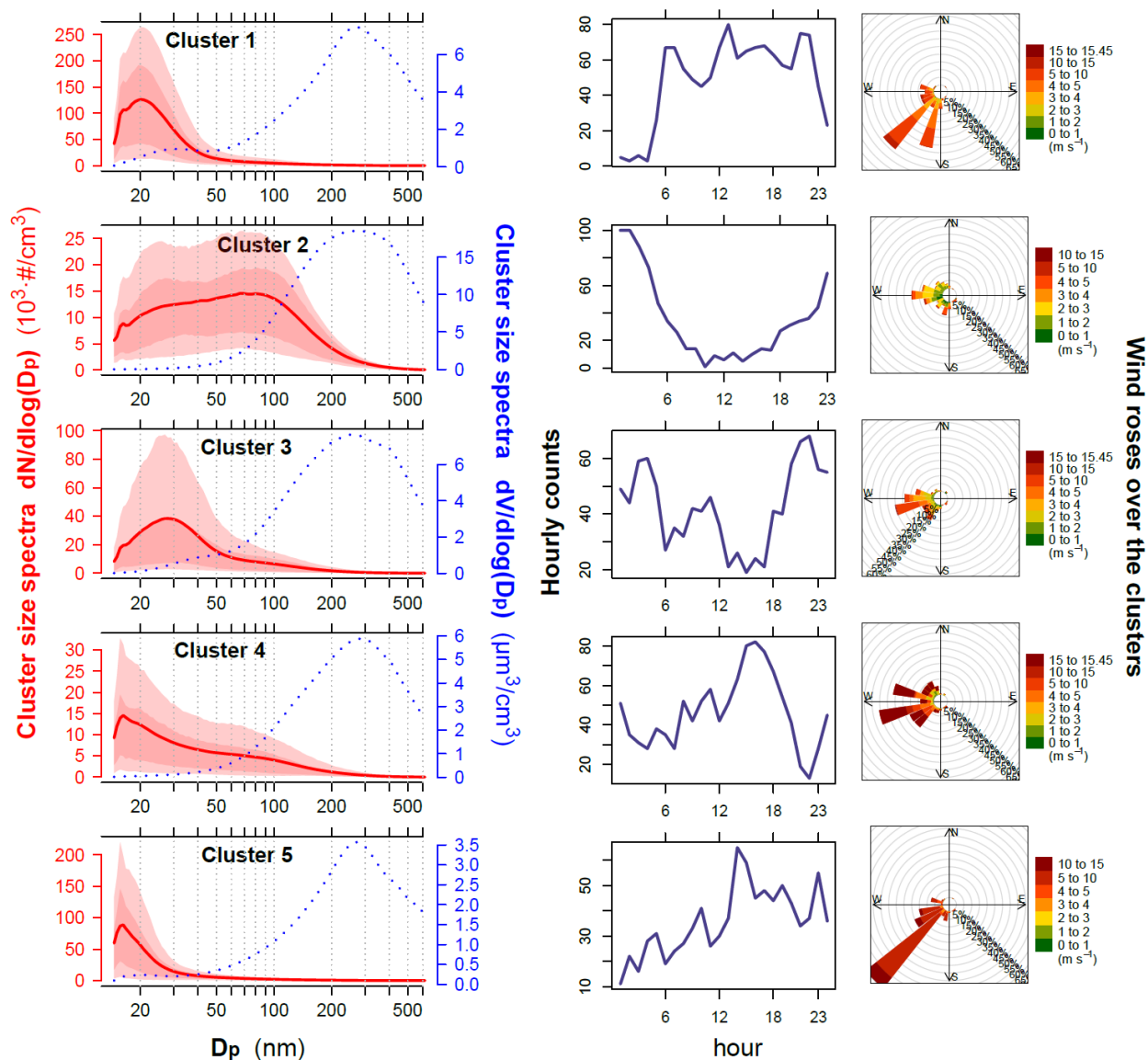


**Figure 4.** Results of cluster analysis for the cold season data. Average cluster PNSD spectra (left) are reported as solid red lines along with: (i) their 10th, 25th, 75th and 90th percentile spectrum as shaded areas; (ii) the volume size distributions (dotted blue line); (iii) the hourly counts and (iv) the wind roses associated with each cluster.

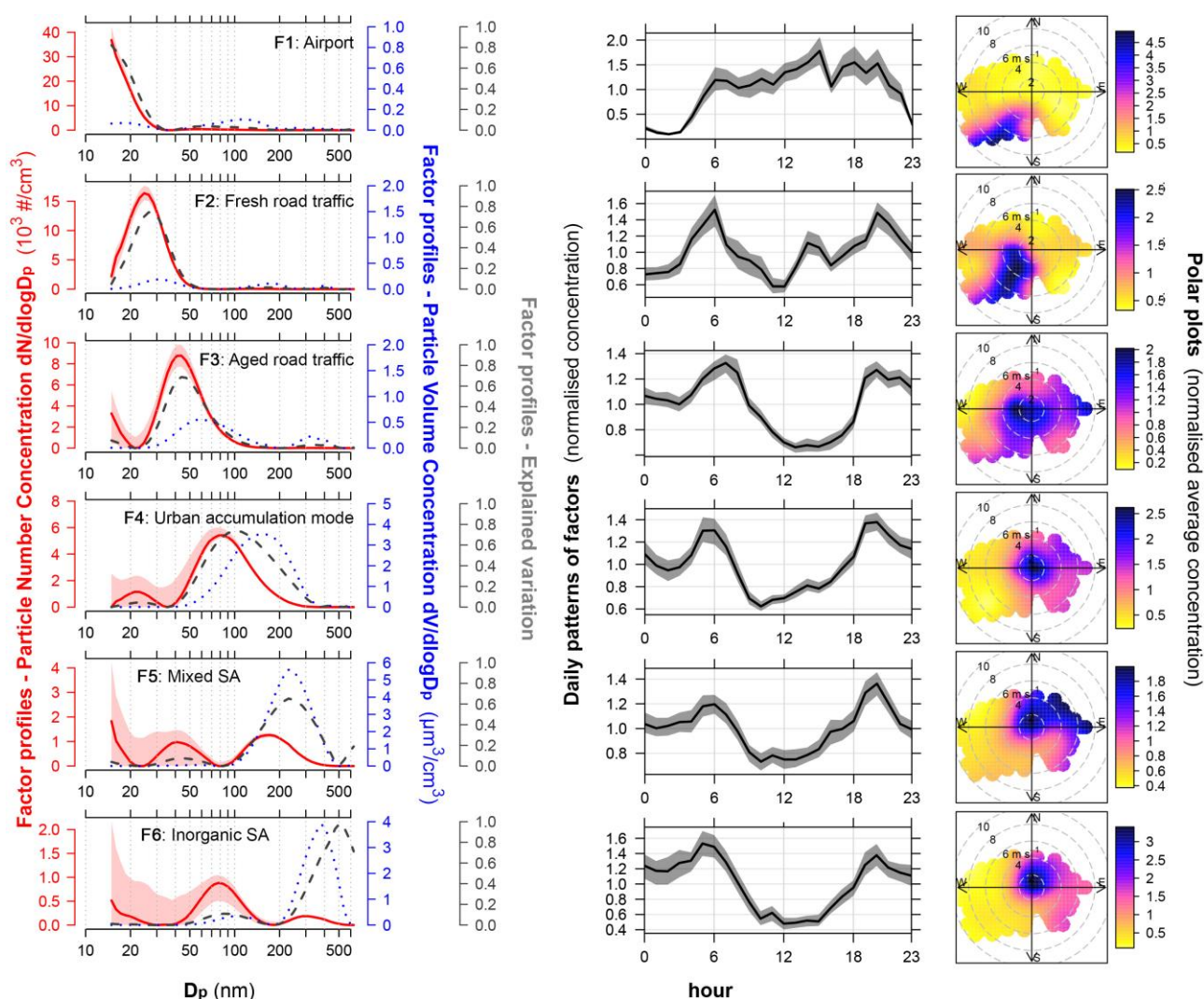


**Figure 5.** Results of PMF analysis for the warm season data. Factor profiles are reported on the left as: (i) number concentration in solid red lines; (ii) their DISP ranges in shaded red areas; (iii) volume concentrations in dotted blue lines; (iv) explained variation in dashed grey lines. The plots on the centre report the normalised daily patterns calculated on the hourly-averaged factor contributions along with their 95th confidence intervals ( $n=200$  bootstrap). The plots on the right show the polar plot analysis (normalised average factor contributions). SA=secondary aerosol.



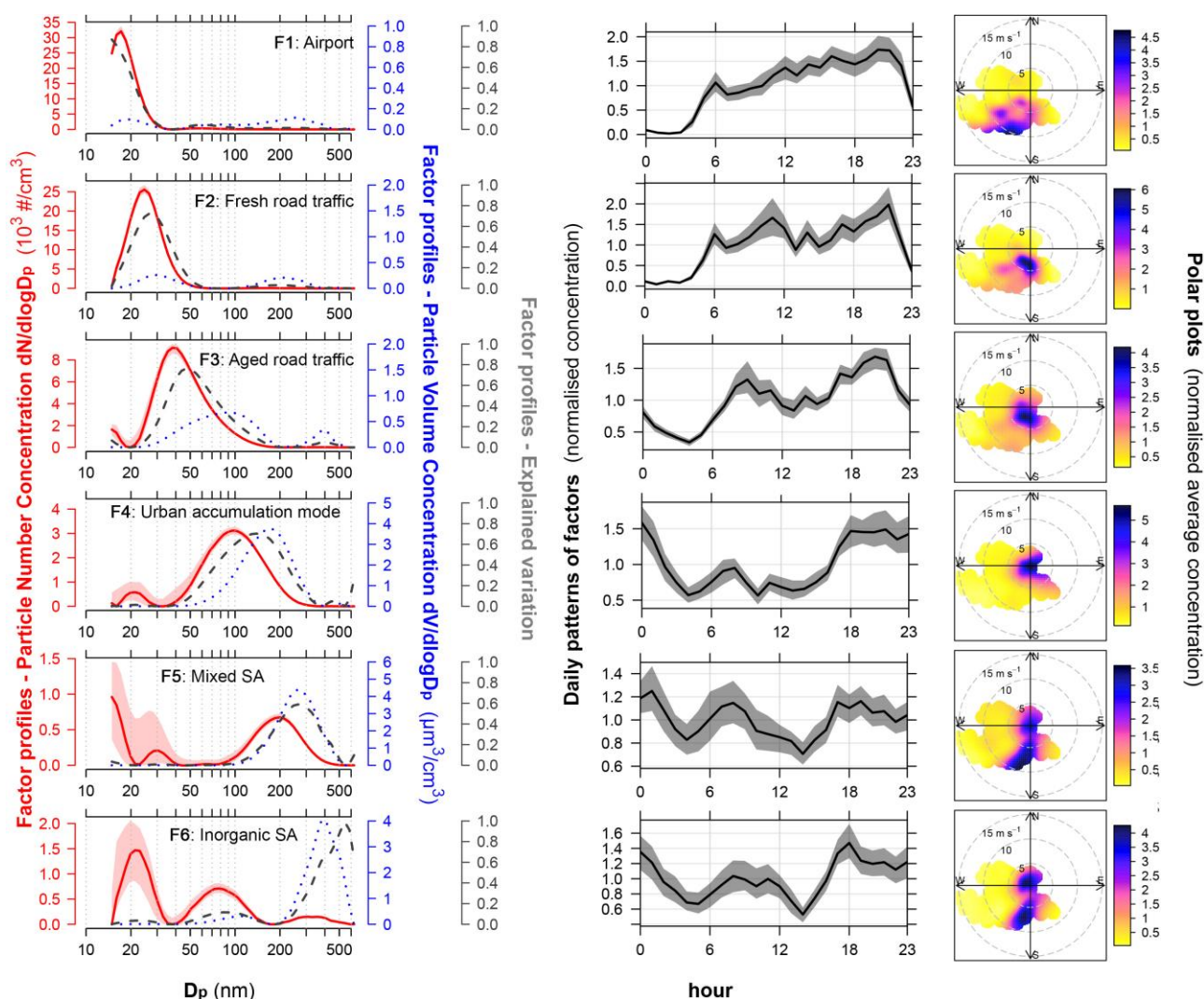


**Figure 6.** Results of PMF analysis for the cold season data. Factor profiles are reported on the left as: (i) number concentration in solid red lines; (ii) their DISP ranges in shaded red areas; (iii) volume concentrations in dotted blue lines; (iv) explained variation in dashed grey lines. The plots on the centre report the normalised daily patterns calculated on the hourly-averaged factor contributions along with their 95th confidence intervals ( $n=200$  bootstrap). The plots on the right show the polar plot analysis (normalised average factor contributions). SA=secondary aerosol.

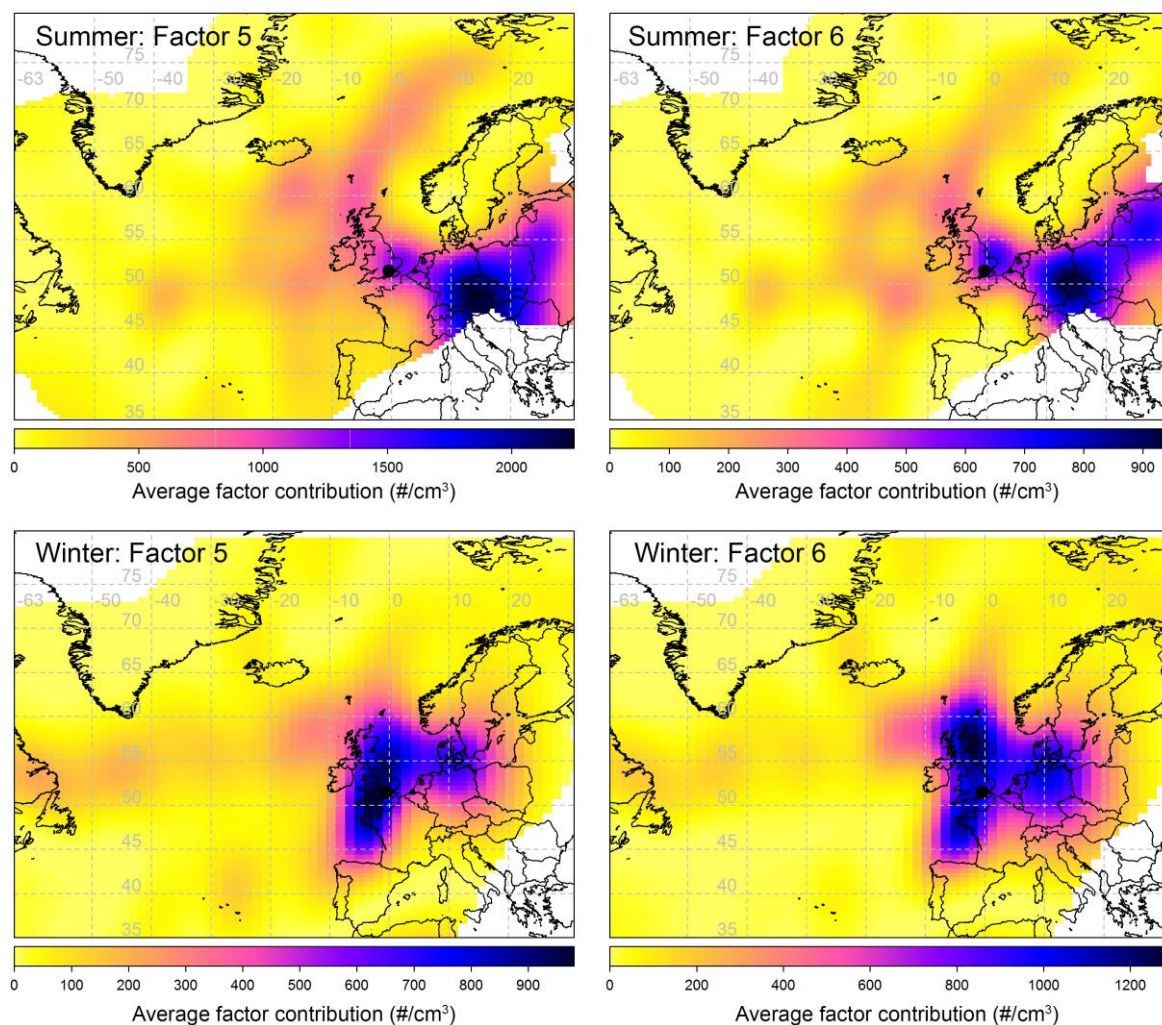
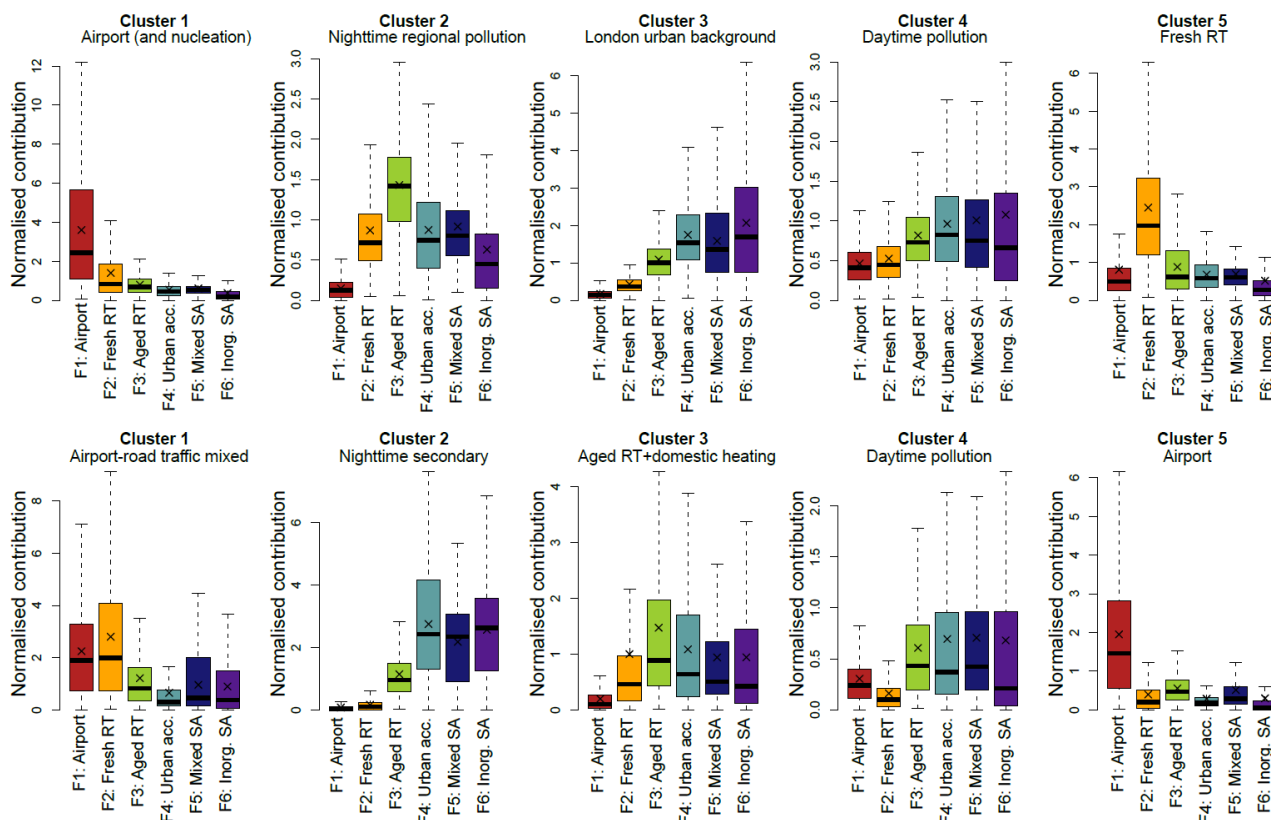


**Figure 7.** CWT maps of the secondary aerosol-related factors for both the seasons. Map scales refer to the average factor contributions to the total variable (PNC).





1552

1553

1554

1555

**Figure 8.** Comparison of k-means and PMF for the warm (upper plots) and cold (bottom plots) seasons. Boxplot statistics: lines= medians, crosses= arithmetic means, boxes= 25th-75th percentile ranges, whiskers=  $\pm 1.5 \times$  inter-quartile ranges.

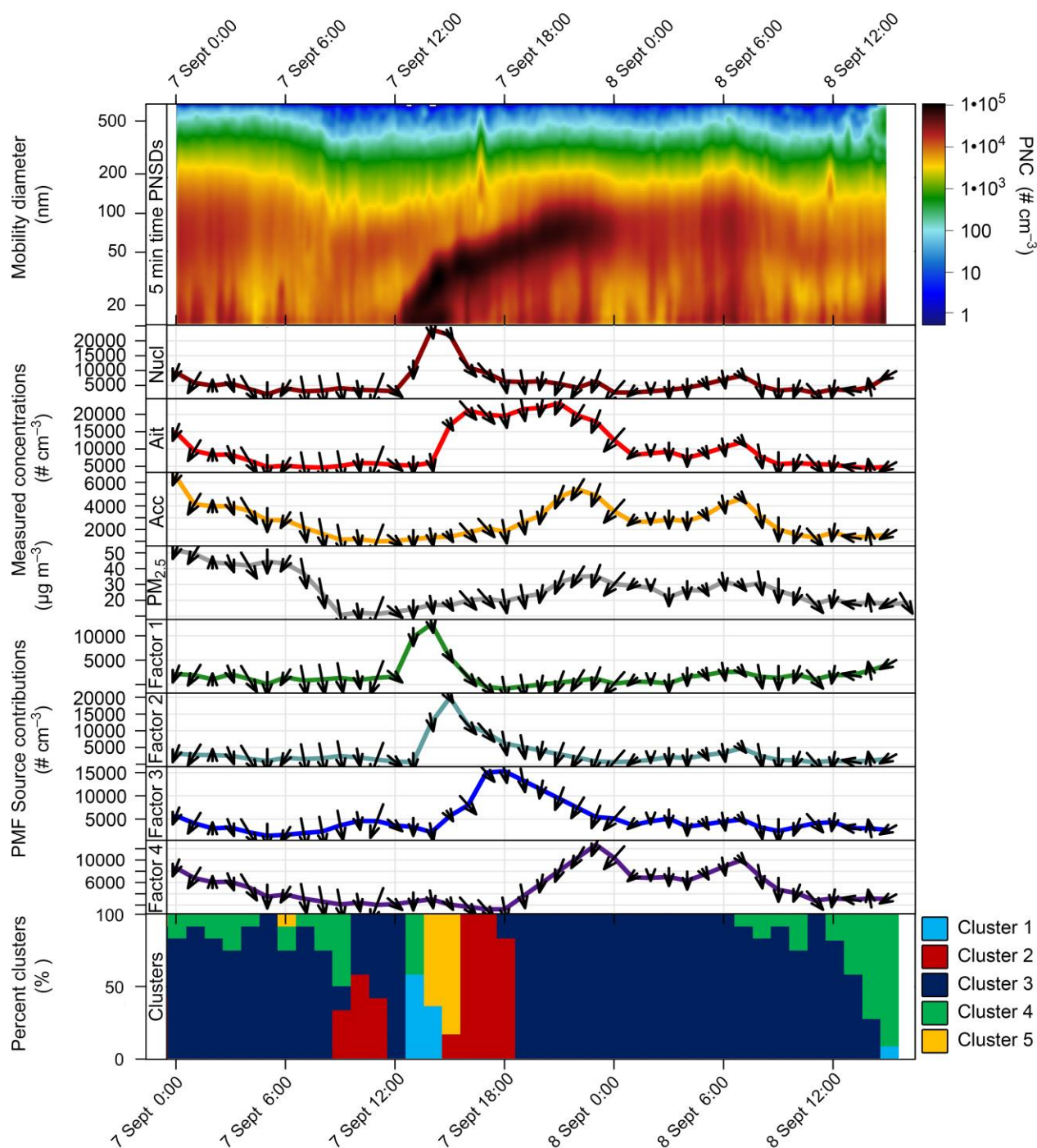


**Figure 9.** Analysis of the regional nucleation episode occurring on September 7th. The selected period is from 7 September midnight to 8 September 4 pm. The plots represent (from upper to the bottom): (a) contour plots of SMPS data; (b) Concentrations of some measured species (Nucl= particles in the nucleation range 14-30 nm; Ait= particles in the Aitken Nuclei range 30-100 nm; Acc= particles in the accumulation range >100 nm; mass of PM<sub>2.5</sub>); (c) Source contributions from PMF for the Factors 1, 2, 3 and 4; (d) hourly counts of number of clusters. The arrows in the (b) and (c) plots show the wind direction (arrow direction) and speed (proportional to arrow length).